Cell Reports

Article

The Diabetes Gene *JAZF1* Is Essential for the Homeostatic Control of Ribosome Biogenesis and Function in Metabolic Stress

Graphical Abstract

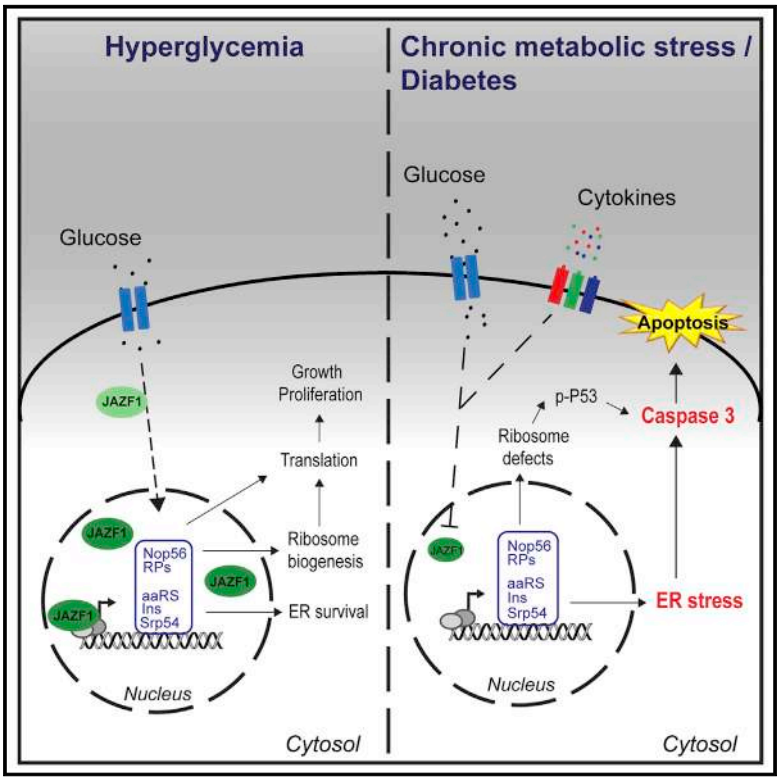

Highlights

- JAZF1 localizes in the nucleus in high-glucose and metabolic stress conditions
- JAZF1 mediates metabolic stress via endoplasmic reticulum and p53 stress pathways
- JAZF1 regulates ribosome biogenesis and aminoacyl-tRNA synthetases
- JAZF1 is a direct negative regulator of insulin gene transcription

Authors

Ahmad Kobiita, Svenja Godbersen, Elisa Araldi, ..., Giatgen Spinas, Holger Moch, Markus Stoffel

Correspondence

stoffel@biol.ethz.ch

In Brief

JAZF1 has been identified in several GWASs as a type 2 diabetes susceptibility gene. Kobiita et al. demonstrate that JAZF1 is a transcriptional regulator that is translocated in the nucleus upon metabolic stress and in diabetes. The study also reveals numerous functions of JAZF1 in the regulation of genes involved in ribosome biogenesis and protein translation, including insulin gene transcription.

Kobiita et al., 2020, Cell Reports *32*, 107846
July 7, 2020
https://doi.org/10.1016/j.celrep.2020.107846

CellPress

Cell Reports

CellPress
OPEN ACCESS

Article

The Diabetes Gene *JAZF1* Is Essential for the Homeostatic Control of Ribosome Biogenesis and Function in Metabolic Stress

Ahmad Kobiita,[1] Svenja Godbersen,[1] Elisa Araldi,[1] Umesh Ghoshdastider,[1] Marc W. Schmid,[2] Giatgen Spinas,[3] Holger Moch,[4] and Markus Stoffel[1,5,6,*]

[1]Institute of Molecular Health Sciences, ETH Zurich, Otto-Stern-Weg 7, HPL H36, 8093 Zürich, Switzerland
[2]MWSchmid GmbH, Möhrlistrasse 25, 8006 Zurich, Switzerland
[3]Klinik für Endokrinologie, Diabetologie und Klinische Ernährung, Universitäts-Spital Zürich, Rämistrasse 100, 8091 Zürich, Switzerland
[4]Department of Pathology and Molecular Pathology, University and University Hospital Zürich, Schmelzbergstrasse 12, 8091 Zürich, Switzerland
[5]Medical Faculty, University of Zurich, Zurich, Switzerland
[6]Lead Contact
*Correspondence: stoffel@biol.ethz.ch
https://doi.org/10.1016/j.celrep.2020.107846

SUMMARY

The ability of pancreatic β-cells to respond to increased demands for insulin during metabolic stress critically depends on proper ribosome homeostasis and function. Excessive and long-lasting stimulation of insulin secretion can elicit endoplasmic reticulum (ER) stress, unfolded protein response, and β-cell apoptosis. Here we show that the diabetes susceptibility gene *JAZF1* is a key transcriptional regulator of ribosome biogenesis, global protein, and insulin translation. JAZF1 is excluded from the nucleus, and its expression levels are reduced upon metabolic stress and in diabetes. Genetic deletion of *Jazf1* results in global impairment of protein synthesis that is mediated by defects in ribosomal protein synthesis, ribosomal RNA processing, and aminoacyl-synthetase expression, thereby inducing ER stress and increasing β-cell susceptibility to apoptosis. Importantly, JAZF1 function and its pleiotropic actions are impaired in islets of murine T2D and in human islets exposed to metabolic stress. Our study identifies JAZF1 as a central mediator of metabolic stress in β-cells.

INTRODUCTION

Glucose-induced insulin secretion (GSIS) from pancreatic β-cells plays a key role in glucose homeostasis. Functional and sufficient β-cells are required to maintain normoglycemia. Genetic and environmental factors as well as aging are major risk factors for the gradual decline in insulin secretion. Genome-wide association studies (GWASs) have revealed a variety of type 2 diabetes (T2D) susceptibility genes, many of which appear to primarily be involved in β-cell differentiation and function (Bonnefond et al., 2010). Three defects have consistently been reported in patients with T2D: gradual decline in β-cell function and dedifferentiation and a reduction in β-cell mass (Accili et al., 2016). The molecular mechanisms of β-cell failure in T2D are incompletely understood, but several lines of evidence suggest that mitochondrial dysfunction (Mulder, 2017), oxidative and endoplasmic reticulum (ER) stress (Keane et al., 2015), dysfunctional fatty acid metabolism (Prentki et al., 2013), glucolipotoxicity (Poitout and Robertson, 2008), and amyloid deposition (Hull et al., 2004) contribute to functional β-cell alterations and loss of β-cell mass by apoptosis and compromised proliferation. The functional adaptation of β-cells and the response to chronic metabolic stress have been linked to ER stress and the unfolded protein response (UPR) (Back and Kaufman, 2012).

Proinsulin biosynthesis is regulated by nutrients, most notably glucose. Short-term glucose stimulation (≤2h) leads to a rapid (~2-fold) increase in total protein synthesis and an ~20-fold increase in proinsulin synthesis (Itoh and Okamoto, 1980). This process is mediated almost entirely by enhanced translation of preexisting mRNAs that are translocated from an inert cytosolic pool to translationally active membrane-bound polysomes on the rough ER, and ultimately through an augmented rate of initiation, facilitated through increased availability of the translational ternary complex and brought about by the dephosphorylation of eIF2α (Scheuner et al., 2005; Sonenberg and Hinnebusch, 2009). Prolonged glucose stimulation also leads to increases in preproinsulin mRNA levels (~2-fold), increased insulin mRNA stability, and a corresponding increase in proinsulin translation (≥10-fold) (Brunstedt and Chan, 1982). However, chronic overproduction of insulin per se (i.e., in insulin resistance) or genetic mutations (e.g., in the insulin gene) can lead to the formation of misfolded proteins that may generate ER stress (Arunagiri et al., 2018). This in turn can trigger intracellular signaling events that ultimately activate transcription of ER chaperones, oxidoreductases, and ER-associated protein degradation (ERAD) components.

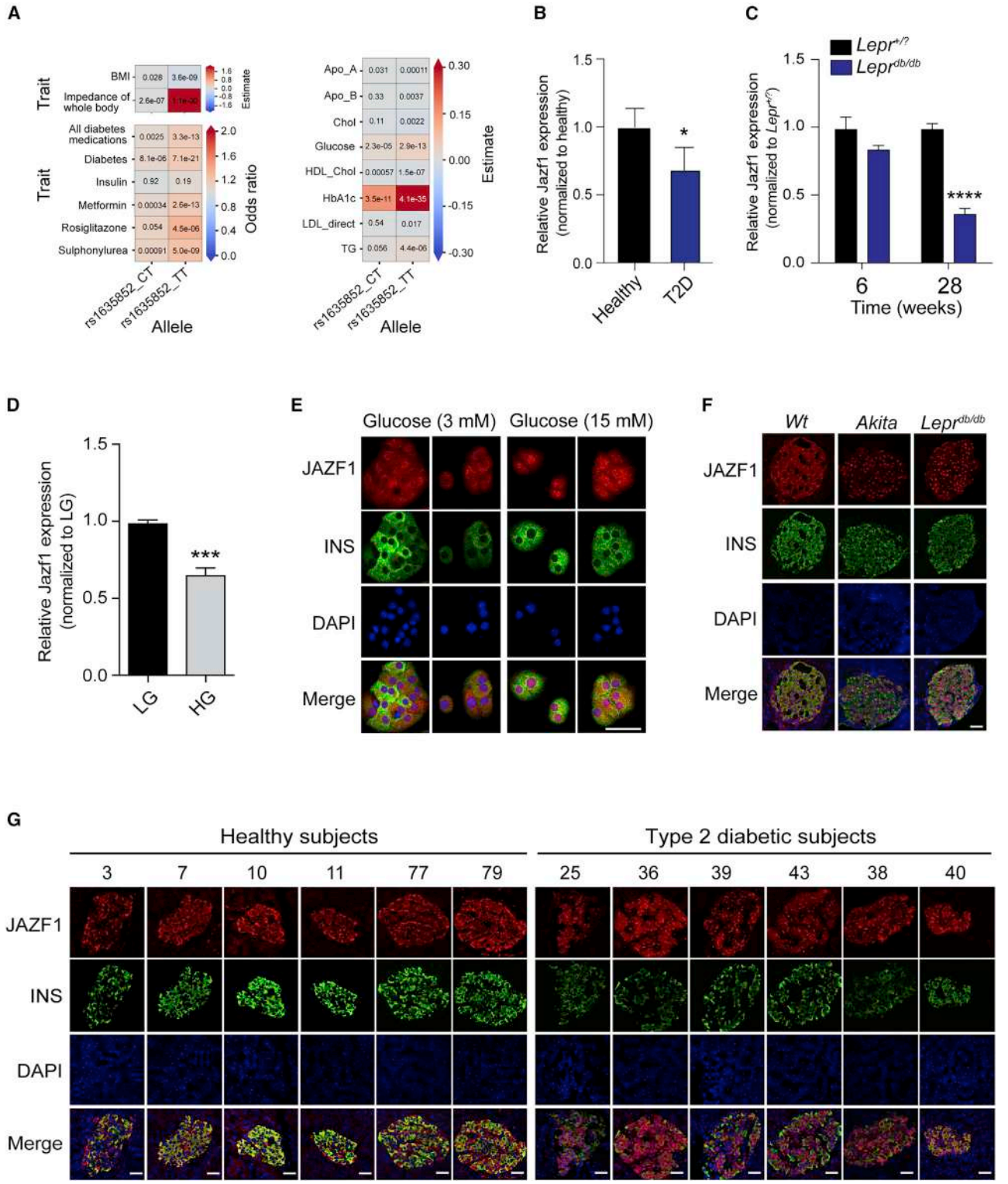

Figure 1. Jazf1 Levels and Localization of β-Cells in Normoglycemia and in T2D

(A) Association analyses of indicated phenotypes and quantitative traits in European-ancestry participants of UK Biobank. p values of associations are indicated, while odds ratio or estimates are color-coded. p values < 5e-8 are significant. Number of participants analyzed per trait ranged between 354,259 and 487,867. (B–D) Expression levels of Jazf1 in islets from healthy humans and T2D patients (n = 5) (B), islets from *Lepr*$^{db/db}$ and control littermate mice at 6 and 28 weeks (n = 3) (C), and mouse islets cultured in 3 mM (LG) and 24 mM (HG) glucose for 24 h (n = 3) (D).

(legend continued on next page)

Normally, this response enhances the cell's capacity to sustain protein secretion during times of high demands. If adaptive UPR outputs are effective, this will lead to a reduction of unfolded proteins and restoration of homeostasis. However, if ER stress persists, the UPR switches its physiological output from promoting adaptation to instead promoting self-destruction, usually through apoptosis (Papa, 2012). The regulation of β-cell gene expression in response to metabolic stress has been extensively studied at the transcriptional level, but regulation of mRNA translation, including ribosome biogenesis and rRNA processing, has received less attention. Likewise, how these processes are regulated transcriptionally and how they may be linked to ER stress and the UPR pathways during the development of T2D is not understood.

Juxtaposed with another zinc finger (ZnF) protein 1, JAZF1 (TIP27, ZNF802) encodes a 27 kDa protein with three C2H2-type ZnFs and functions as a repressor of DNA response element 1 (DR1)-dependent transcription of nuclear receptor subfamily 2, group C, member 2 (NR2C2, TR4) (Nakajima et al., 2004). JAZF1 represses NR2C2 transcriptional activity via direct binding to the ligand-binding domain (LBD) of NR2C2 (Omori et al., 2005; Lee et al., 1997; Tanabe et al., 2007).

GWASs have identified gene variants in that are linked to insulin secretion and increased susceptibility to develop T2D (Grarup et al., 2008; Zeggini et al., 2008). JAZF1 levels are decreased in pancreatic islet of T2D patients, and increased transcript levels are associated with higher insulin secretion (Taneera et al., 2012). Gene variants involving JAZF1 are also associated with height (Manolio, 2010), risk for prostate cancer (Thomas et al., 2008), and endometrial stromal tumors (Koontz et al., 2001). Although NR2C2 may have functions in energy homeostasis and inflammation (Liu et al., 2007; Kang et al., 2011; Yang et al., 2014; Meng et al., 2018), no studies have explored its role in pancreatic β-cells, except a recent study demonstrating allele-specific transcriptional activity at T2D-associated single-nucleotide polymorphisms in regions of open chromatin at the JAZF1 locus (Fogarty et al., 2013).

In this study we used genetic, molecular, biochemical, and physiological approaches to investigate the role of JAZF1 in islet gene regulation and report a previously unrecognized role as an essential regulator of mRNA translation through coordinating protein gene expression, ribosome biogenesis, and rRNA processing. We further show that impaired JAZF1 function in T2D contributes to ribosomal and ER stress, activation of apoptosis pathways, and ultimately β-cell demise.

RESULTS

Genetic *JAZF1* Variance, Decreased JAZF1 Expression, and Nuclear JAZF1 Localization in Pancreatic β-Cells Are Associated with T2D and Metabolic Stress

We studied an intronic variant in the *JAZF1* gene (rs1635852; pairwise $R^2 < 0.01$, minor allele frequency in dataset 49.63%), that has been shown to display allelic differences in enhancer activity with the T2D risk allele T showing lower transcriptional activity (Fogarty et al., 2013). Genotypes from ~400,000 European-ancestry participants from UK Biobank, a U.K. population-based cohort of people 40–69 years of age (Bycroft et al., 2018), were analyzed to confirm that variations in the *JAZF1* genomic locus predispose to T2D, as shown by significant associations of the rs1635852_TT genotype with diabetes phenotypes and traits. Interestingly, the association of the risk genotype with lower body mass index indicates that JAZF1 may have a key role in β-cell function rather than in organs regulating insulin sensitivity and energy homeostasis (Figure 1A).

We first examined the expression of Jazf1 across metabolic tissues in mice fed with a chow diet. We found that Jazf1 transcript levels were most abundant in pancreatic islets, followed by adipose tissue, where expression was previously reported to be highest in all tissues (Figure S1A) (Ho et al., 2013; Yang et al., 2015).

Several studies have shown that Jazf1 mRNA is decreased in T2D islets and that increased transcript levels are associated with higher insulin secretion (Taneera et al., 2012). Indeed, we found reduced JAZF1 expression in human islets from T2D organ donors compared with healthy donors (Figure 1B). Furthermore, in $Lepr^{db/db}$ compared with control $Lepr^{+/?}$ mice, Jazf1 transcript levels were slightly decreased at 6 weeks of age and reduced by more than 2-fold at 28 weeks of age, at which time $Lepr^{db/db}$ mice became profoundly diabetic (Figure 1C). Pancreatic mouse islets from wild-type (WT) mice cultured in high-glucose conditions also had decreased Jazf1 levels (Figure 1D). Last, we found that Jazf1 expression was decreased in islets of patients with type 1 diabetes (T1D) and in a mouse model of T1D (NOD) (Figures S1B–S1D).

Jazf1 has a putative nuclear localization sequence (NLS), located within the second ZnF motif (Figure S1E). We noticed a significant homology of the C-terminal ZnF motif between JAZF1 and yeast Sfp1 (Figure S1F), a transcription factor that controls the expression of more than 60 genes involved in ribosome biogenesis, cell cycle G2/M transition, and DNA damage response (Fingerman et al., 2003; Albert et al., 2019). Immunofluorescence staining revealed nuclear localization in transformed rat and human β-cell lines exposed to low and high glucose, indicating a role in proliferation (Figures S1G and S1H), a notion that was supported by reduced cell division when Jazf1 was silenced (Figure S1I). In primary β-cells, JAZF1 was localized mostly in the cytosol at low glucose but translocated to the nucleus at high glucose levels (Figure 1E). Similarly, we observed a predominant cytosolic distribution of JAZF1 in WT mice fed *ad libitum* a chow diet. In contrast, JAZF1 was located mainly in the nuclei of β-cells from hyperglycemic *Akita* and $Lepr^{db/db}$ mice, in which T2D develops as a result of ER stress due to a mutation in *Ins2* and severe insulin resistance, respectively (Figure 1F). This finding was confirmed by subcellular fractionation and immunoblotting experiments in islets of $Lepr^{db/db}$ and control mice (Figure S1J).

(E–G) Immunohistochemistry of isolated mouse β-cells cultured in low (3 mM) and high (15 mM) glucose for 1 h (E), pancreatic sections of wild-type (WT), *Akita*, and $Lepr^{db/db}$ mice (24 weeks of age) (F), and pancreatic biopsies of six healthy and six T2D human subjects (G), stained for JAZF1, Insulin, and DNA (DAPI). Scale bars: 25 μm (E) and 100 μm (E–G). Numbers in (E) and (G) represent anonymized identifiers. Clinical data of human subjects (G) is shown in Figure S1K. Data are presented as mean ± SD. *$p \leq 0.05$, **$p \leq 0.01$, and ***$p \leq 0.001$ by Student's t test.

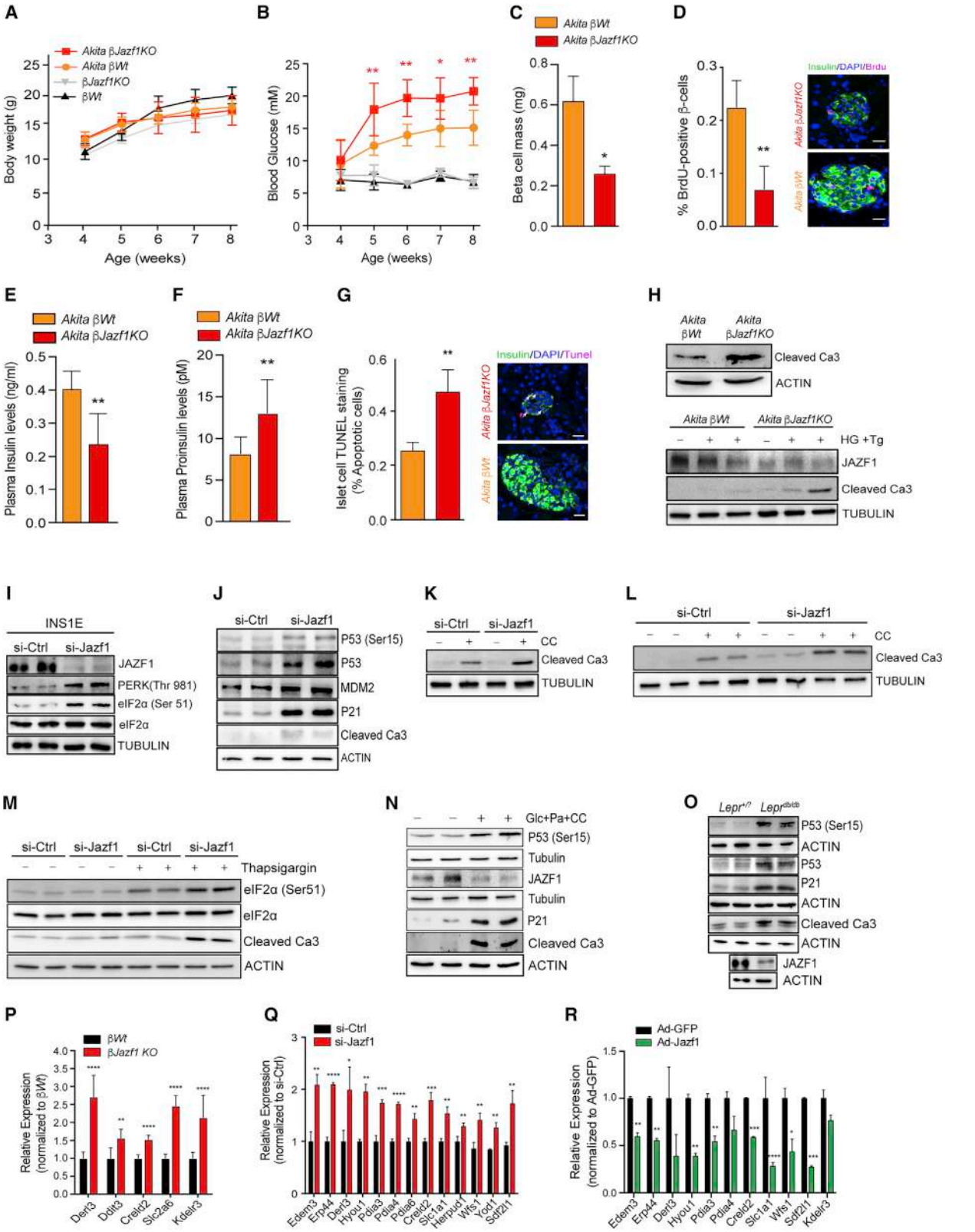

(legend on next page)

We also found that JAZF1 was preferentially localized in the nuclei of β-cells in pancreatic tissue sections of human T2D subjects, whereas it localized mainly to the cytosol of non-diabetic controls (Figures 1G and S1K). Last, in contrast to JAZF1, NR2C2 was always associated with the nucleus, irrespective of the glucose levels, in primary β-cells or in *Akita* mice (Figures S1L and S1M). These results demonstrate that JAZF1 expression levels and cellular compartmentalization are regulated by metabolic stress conditions, leading to a nuclear localization in response to elevated glucose concentrations.

Increased Susceptibility of JAZF1-Depleted β-Cells to ER Stress-Induced Apoptosis

To study the function of JAZF1, we generated β-cell-specific Jazf1 knockout mice by crossing *Jazf1*$^{fl/fl}$ mice with *RIP-Cre* transgenic mice that express Cre-recombinase under the control of the rat insulin 2 promoter (called *βJazf1KO*). PCR and western blot analysis confirmed the specific ablation of Jazf1 in islets but not in other metabolic tissues (Figures S2A–S2C). *βJazf1KO* mice were indistinguishable from control *Jazf1*$^{fl/fl}$ littermates (called *βWt*) with regard to weight, blood glucose, and GSIS in isolated islets (Figures S2D–S2F). Pancreatic insulin content and β-cell mass were reduced in *βJazf1KO* mice at age 16 weeks compared with *βWt* mice, with a similar percentage of Ki-67-positive β-cells (Figures S2G–S2I). Challenging animals with a high-fat diet (HFD) for 12 weeks resulted in a similar phenotype with regard to weight, blood glucose, and glucose tolerance (Figures S2J–S2L). Similar to chow-fed mice, *βJazf1KO* animals on the HFD had reduced β-cell mass and displayed lower β-cell proliferation compared with *βWt* mice (Figures S2M and S2N).

We next studied the consequences of genetic *Jazf*1 ablation in *Akita* mice, a well-characterized genetic T2D model, due to unresolved ER stress and β-cell apoptosis (Yoshioka et al., 1997; Wang et al., 1999). *Akita βJazf1KO* mice exhibited similar body weight but higher blood glucose levels compared with *Akita βWt* mice (Figures 2A and 2B). The β-cell mass was reduced by 50% in *Akita βJazf1KO* mice (Figure 2C), and measurements of β-cell proliferation by *in vivo* BrdU assays showed a ~70% reduction compared with *Akita βWt* mice (Figure 2D). Furthermore, plasma insulin levels were decreased and proinsulin levels increased in *Akita βJazf1KO* animals (Figures 2E and 2F), with no changes in the levels of insulin-processing genes (Pcsk1, Pcsk2, Cpe) (Figure S2O).

Unresolved ER stress can lead to β-cell death through the activation of p53-dependent apoptotic pathways in murine (Hoshino et al., 2014) and human (Tornovsky-Babeay et al., 2014) T2D. We performed TUNEL staining and cleaved caspase-3 assays and found that β-cell apoptosis was increased in 8-week-old *Akita βJazf1KO* mice compared with *Akita* control animals (Figures 2G and 2H). A similar response was observed when challenging islets of *Akita βJazf1KO* with high glucose for 24 h, followed by thapsigargin (TG) treatment for 5 h (Figure 2H). Interestingly, knockdown of Jazf1 in INS1E cells was sufficient to activate ER stress genes PERK and eIF2a (Figure 2I) as well as the p53 pathway, as measured by increased phosphorylation of p53(Ser15), p53 accumulation, and activation of its targets P21 and MDM2, in unstressed conditions (Figure 2J).

We next studied the response of Jazf-depleted INS1E and MIN6 cells to various stresses: treatment of cells with a cytokine cocktail (CC) or TG, which are known to induce ER dysfunction and initiate cell death (Cardozo et al., 2005; Lerner et al., 2012), led to increased Ser51 phosphorylation of eIF2a and more apoptosis as shown by higher levels of cleaved caspase-3 compared with si-Ctrl-transfected cells (Figures 2K–2M). Of note, the expression of JAZF1 protein levels decreased in human primary islets exposed to a diabetogenic milieu (high glucose, palmitic acid, and cytokines) (Figure 2N). Furthermore, JAZF1 levels also decreased in islets exposed to ER stress (Figure 2H) and to INS1E cells treated with TG (Figure S2P). These results are also consistent with increased ER stress markers in islets from *Lepr*$^{db/db}$ mice that are known to undergo ER stress-induced apoptosis (Figures 2O and S2Q). Interestingly, silencing Nr2c2 in β-cells conferred protection to ER stress (Figures S2R and S2S). Of note, Nr2c2 levels were unaffected in β-cells with induced ER stress (Figure S2T). Taken together, these data provide a link between JAZF1/NR2C2 complex and ER stress in pancreatic β-cells.

When protein production exceeds the ER processing capacity or mutant proteins such as *Ins2Akita C96Y* are not properly folded, they can activate a signaling network called the UPR. The transcriptome analysis of islets from *βJazf1KO* and *βWt* mice identified increased levels of several UPR genes that

Figure 2. Loss of JAZF1 Function in β-Cells Exacerbates ER Stress and Apoptosis *In Vivo* and *In Vitro*

(A–G) Body weight (A), blood glucose levels (B), pancreatic β-cell mass (C), TUNEL staining of insulin-positive islet cells (D), percentage of BrdU-positive β-cells (E), plasma insulin levels (F), and proinsulin levels (G) in mice with indicated genotypes. Islet measurements (C–G) were carried out in 8-week-old mice. In (A), (B), (F), and (G), n = 6 for each group; in (D) and (E)(n = 3). Scale bar: 25 μm.

(H) Immunoblot analysis of cleaved caspase in isolated islets from *Akita βJazf1KO* and *Akita βWt* littermates of 8-week-old animals (top) and after culturing in 24 mM glucose (HG) and TG for 5 h (bottom). Anti-tubulin antibodies were used as a loading control (n = 3). Scale bar: 25 μm.

(I and J) Immunoblot analysis of indicated (phospho) proteins from INS1E cells transfected with siRNAs targeting Jazf1 (si-Jazf1) or control (si-Ctrl) to measure ER stress (I) and p53 pathway activation and apoptosis (J).

(K–M) Immunoblot analysis of cleaved caspase-3 from INS1E (K) and MIN6 (L and M) cells transfected with siRNAs targeting Jazf1 and exposed to a cytokine cocktail (CC; IL-1β, IFN-γ, and TNF-α) for 24 h (K and L) or thapsigargin (M) for 5 h.

(N) Immunoblot analysis of indicated proteins from human pancreatic islets that were exposed to high glucose (Glc), palmitic acid (Pa), and a cytokine cocktail (CC) for 72 h.

(O) Western blot analysis of indicated proteins from isolated pancreatic islets of 28-week-old *db/db* (*Lepr*$^{db/db}$) or control (*Lepr*$^{+/?}$) mice. Each line represents pooled islets from three mice.

(P–R) Transcript levels of UPR-related genes from isolated islets of *βJazf1KO* and control mice (P), INS1E cells transfected with siRNAs targeting Jazf1 (si-Jazf1) or control (si-Ctrl) (Q), or INS1E cells infected with control or Jazf1-expressing adenoviruses (R). n = 3 per group.

Data are presented as mean ± SD. *p ≤ 0.05, **p ≤ 0.01, and ***p ≤ 0.001 by two-way ANOVA with Holm-Sidak multiple-comparisons test (A and B) or Student's t test (C–G and P–R).

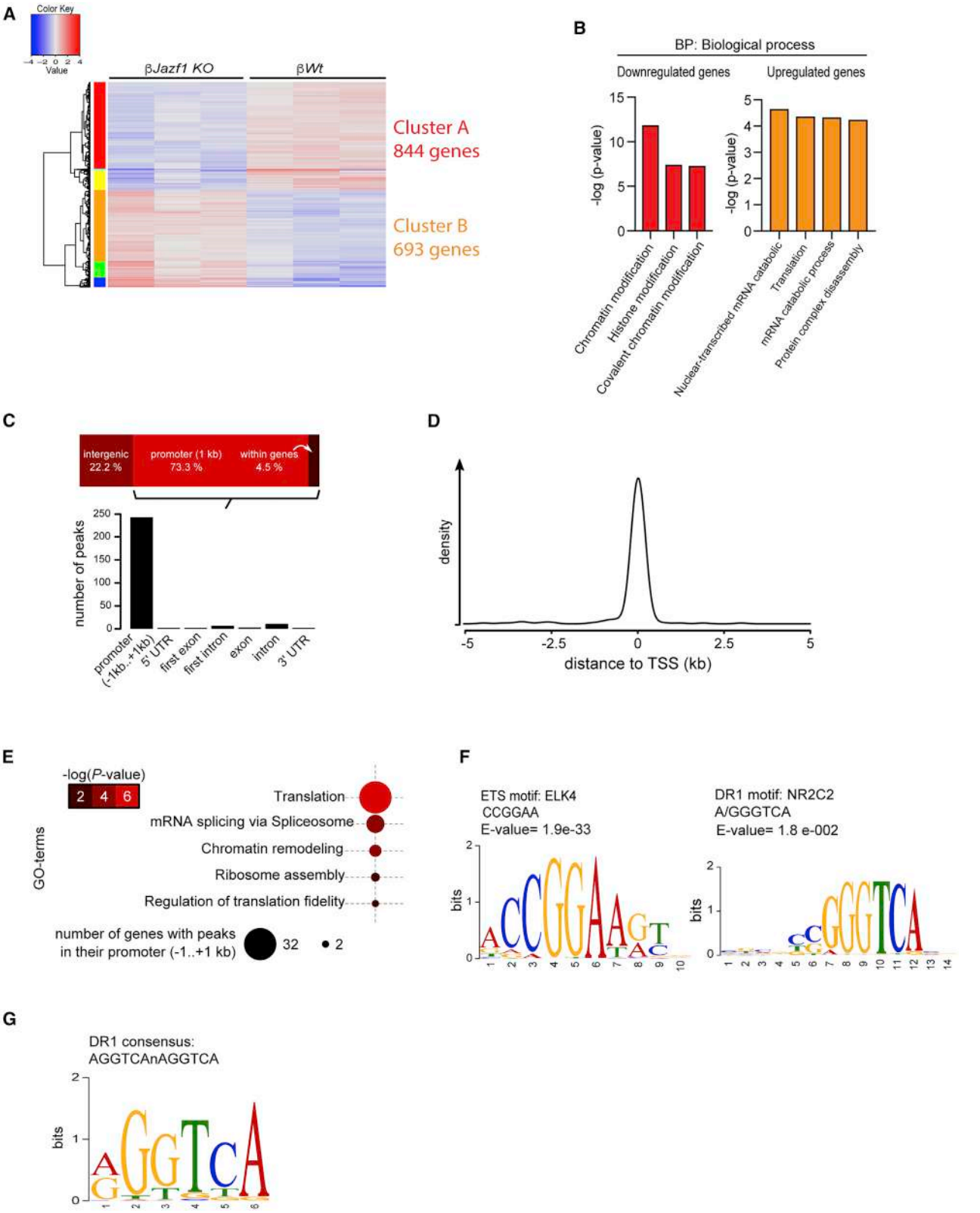

(legend on next page)

included Derl3, Creld2, Kdelr3, and the ER stress gene Ddit3 (Chop) (Figure 2P). One of the most upregulated ER stress-related genes was Derlin-3, which is essential for the machinery of the ERAD pathway by targeting misfolded proteins upon ER stress (Oda et al., 2006). We measured increased levels of several UPR-related genes upon knockdown of Jazf1 in INS1E cells in untreated as well as TG-treated cells (Figures 2Q and S2U). Importantly, overexpression of Jazf1 in primary dispersed mouse islets (Figure 2R) or in INS1E cells (Figure S2V) in high-glucose conditions revealed the opposite transcriptional response. Furthermore, the same genes were upregulated in islets of diabetic *db/db* mice (Figure S2W). These results demonstrate a role of JAZF1 in ER stress responses and indicate that decreased JAZF1 expression in β-cells may contribute to the activation of ER stress pathways and ultimately apoptosis.

Genome-wide Identification of JAZF1 Targets by RNA and ChIP Sequencing

In search of a molecular explanation for the ER stress/apoptosis susceptibility of *Jazf1*-deficient β-cells, we performed RNA sequencing (RNA-seq) on isolated islets of *βJazf1KO* and *βWt* mice (Table S1). The transcriptome analysis identified 2,637 significantly regulated genes with mild gene expression changes ($\log_2$ fold change $\leq$ 0.5, p $\leq$ 0.01, false discovery rate [FDR] < 0.05) upon deletion of *Jazf1* (Figure S3A). Hierarchical clustering on the basis of RNA levels identified two major gene sets (Figure 3A), with 844 downregulated genes (cluster A) and 693 upregulated genes (cluster B) in *βJazf1KO* islets compared with *β Wt* littermates. Gene Ontology (GO) analysis of cluster A identified enriched annotated gene products relating to histone and chromatin modification (Figure 3B). Gene set B showed GO enrichment in nuclear-transcribed mRNAs, mRNA catabolic processes, and protein translation (Figure 3B). These results are consistent with JAZF1 as a principal transcriptional regulator of ribosome biogenesis and functional ortholog of Sfp1.

To confirm the transcriptional role of JAZF1 at the chromatin level, we performed a genome-wide chromatin immunoprecipitation (ChIP) sequencing (ChIP-seq) analysis of JAZF1 in pancreatic β-cells. Because no suitable antibody for ChIP was available, we infected cells with a recombinant adenovirus expressing HA-tagged JAZF1 at a low MOI to perform ChIP. After 24 h, Jazf1 transcript and protein levels were increased ~2.5-fold compared with endogenous Jazf1 levels (Figures S3B and S3C). ChIP analysis identified 316 target genes that were enriched mainly for proximal promoter regions (Figure 3C), as shown by the majority of JAZF1 peaks occurring within 1 kb relative to the transcription start site (TSS) (Figure 3D; Table S2). To identify putative biological processes for JAZF1 targets, we carried out an enrichment analysis for GO and Kyoto Encyclopedia of Genes and Genomes (KEGG) analysis and found that Jazf1 targets were enriched for biological processes such as translation, ribosome, mRNA splicing, chromatin remodeling, and regulation of translation fidelity (Figures 3E and S3D). In line with our RNA-seq data, the ChIP-seq analysis also supported JAZF1's role as a transcriptional regulator of ribosome biogenesis and protein synthesis. Because sequence-specific DNA binding domains for JAZF1 have not been identified, we used the *de novo* motif discovery program MEME-ChIP (Machanick and Bailey, 2011) to identify sequence motifs that are overrepresented in JAZF1 binding sites. The most significant JAZF1-associated motifs corresponded to consensus binding sites for the ETS domain family transcription factors (E26 transformation specific), which are unique to metazoans (Degnan et al., 1993). Of the 243 JAZF1 promoter binding sites, 63% contain at least one ETS consensus motif CCGGAA (Figure 3F). ETS family transcription factors interact with a multitude of co-regulatory partners to elicit gene-specific responses and drive distinct biological processes such as development, cell cycle, proliferation, and apoptosis (Oikawa and Yamada, 2003). Additionally, JAZF1 has been shown to function as a repressor of the direct repeat DNA element (DR1)-dependent transcriptional regulation by Nr2c2 through interaction with its LBD (Nakajima et al., 2004). Nr2c2 has been implicated in both transcriptional activation and repression and comprises the most abundant nuclear hormone receptor (NHR) in pancreatic islets (Bookout et al., 2006; Chuang et al., 2008). To examine the potential interaction between JAZF1 and NR2C2, we performed immunoprecipitation followed by mass spectrometry (IP-MS) in INS1E cells. IP-MS identified only NR2C2 interacting with JAZF1 (Figure S2E; Table S3), a finding that was validated with co-immunoprecipitation assays (Figure S2F). To identify NR2C2 elements in the promoters of JAZF1 target, we used the NHR computational analysis program "NHR-scan" to predict NHR binding sites in genomic sequences (Sandelin and Wasserman, 2005). This analysis revealed that the DR1 motif was overrepresented in the promoters of JAZF1 targets, with 29% of the peaks compared with other NHR motifs (Figure 3G). The DR1 motif in JAZF1 binding sites was also confirmed with MEME analysis (Figure 3F) and confirms ChIP-seq studies of NR2C2 in four different non-β-cell lines that identified a DR1 motif in 30% of peaks (O'Geen et al., 2010). Furthermore, GO analysis of NR2C2 target genes was enriched in ribosome, translation, and RNA processing, similar to our ChIP analysis of JAZF1 targets. Together, the integration of experimental MS-IP, RNA-seq, and ChIP-seq data of JAZF1 and published NR2C2 ChIP data (O'Geen et al., 2010) demonstrates that the JAZF1/NR2C2 complex is a key transcriptional regulator of ribosome biogenesis and protein translation.

Figure 3. JAZF1 Regulates Ribosomal Proteins and Aminoacyl-tRNA Synthetases

(A) Heatmap for hierarchical clustering of differential gene expression in isolated pancreatic islets from *βJazf1KO* and *βWt* mice (n = 3).

(B) Functional enrichment analysis of JAZF1 target genes on the basis of Gene Ontology terms for biological process (BP) of clusters A and B of RNA-seq data from isolated islets from *βJazf1KO* and *βWt* mice.

(C) Representative diagram indicating the distribution of JAZF1 peaks in the genome.

(D) Distribution profile of peak distances relative to the transcription start site (TSS).

(E) Gene Ontology analysis of JAZF1 target genes.

(F and G) Motif analysis of JAZF1 binding site using MEME (F) and NHR scan analysis (G).

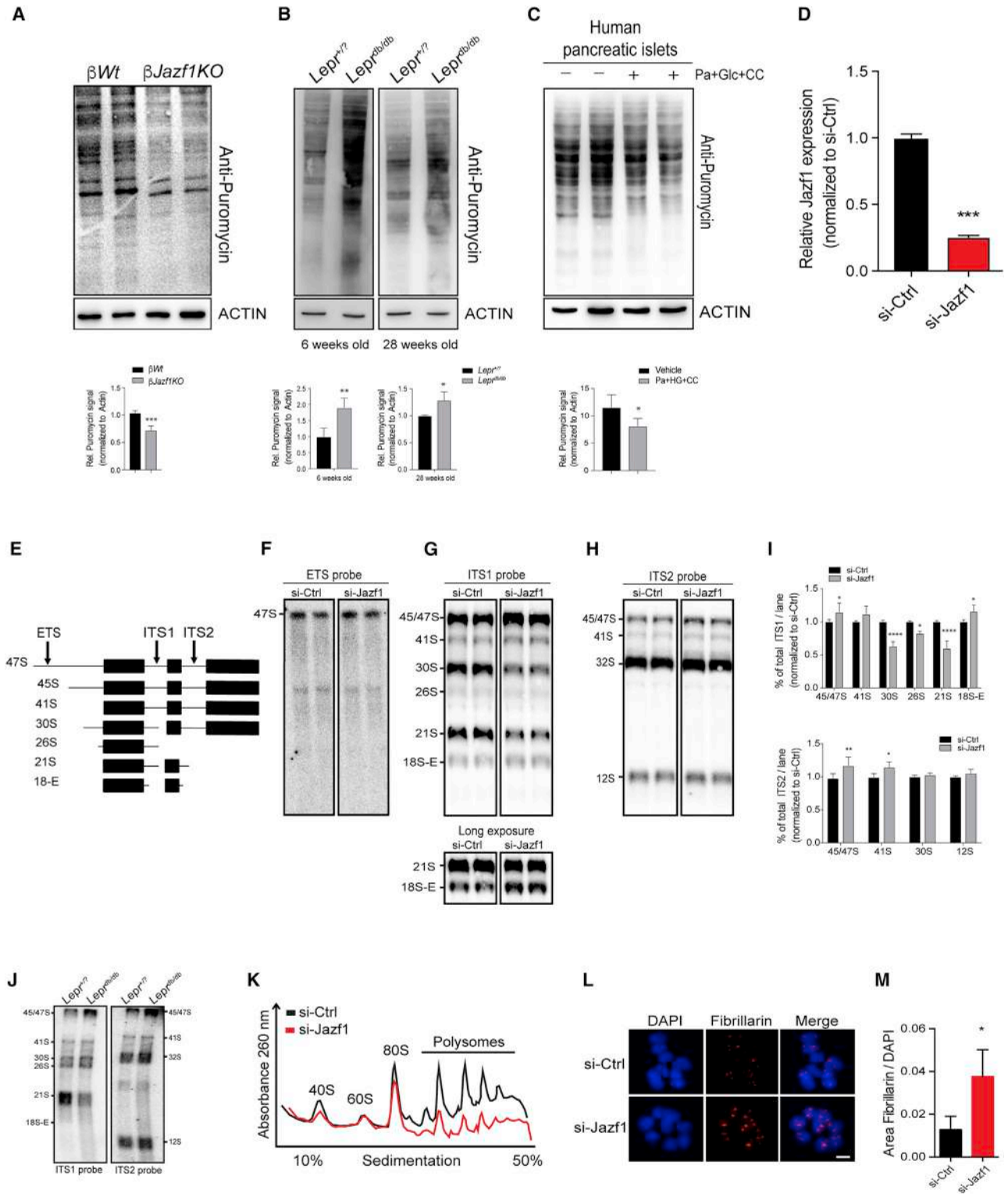

Figure 4. Loss of JAZF1 Function Leads to Impaired Protein Synthesis and rRNA Processing

(A–C) Protein synthesis, assessed via puromycin labeling, in islets of *βJazf1KO* and *βWt* control mice (A), *Lepr*$^{db/db}$ and littermate controls at 6 and 28 weeks of age (B), and human pancreatic islets cultured in the presence or absence of palmitate and cytokines (IL-1β, IFN-γ, and TNF-α) for 72 h (C). Quantifications of total puromycin protein levels normalized to actin; a total of four replicates (A and C) and three replicates (B) are shown below the images.

(D) Jazf1 expression in MIN6 cells following siRNA transfection and determined by qPCR (n = 3).

(legend continued on next page)

Impaired Protein Synthesis and rRNA Processing in *Jazf1*-Null Mice

To investigate JAZF1's involvement in protein synthesis and ribosome biogenesis, we treated islets of *βJazf1KO* and control mice with puromycin and measured the rate of protein synthesis on the basis of the incorporation of puromycin to newly synthesized proteins (Schmidt et al., 2009). Western blot analysis showed decreased levels of translation in islets of *βJazf1KO* compared with *βWt* mice (Figure 4A). We also studied islets of prediabetic and diabetic $Lepr^{db/db}$ mice at the ages of 6 and 28 weeks, respectively, and found increased protein synthesis at 6 weeks of age, when β-cells compensate for insulin resistance by hypersecretion of insulin and β-cell replication (Cavaghan et al., 2000; Rhodes, 2005). However, at 28 weeks of age, the ratio of protein synthesis in $Lepr^{db/db}$ islets was decreased compared with 6-week-old $Lepr^{db/db}$ mice (Figure 4B). These age-dependent alterations in protein synthesis correlate with the well-known compensatory and decompensatory phases of β-cells in diabetes development (Weir and Bonner-Weir, 2004). The data are also in consistent with the profound decrease in protein translation when β-cells are exposed to experimental ER stress (Figure S4A). Protein synthesis was also decreased in human islets that were exposed palmitic acid and a CC and high-glucose conditions for 72 h (Figure 4C). These results demonstrate that JAZF1 expression or activity is required for normal translation of β-cell proteins in physiological and metabolic stress conditions.

We next asked whether JAZF1 might be involved in ribosome biogenesis, thereby providing mechanistic insights linking loss of JAZF1 function and altered protein synthesis. This possibility was tested by silencing JAZF1 in MIN6 cells using small interfering RNAs (siRNAs), leading to a ~80% reduction of Jazf1 transcript levels (Figure 4D), and assessing the processing of the ribosomal subunit precursor RNAs by northern blotting using three different probes: ETS (transcription of 47S rRNA), ITS1 (processing of 18S), and ITS2 (processing of 28S) (Figure 4E). We found that the transcription of 47S rRNA was not affected in Jazf1-depleted cells versus control cells (Figure 4F), but the ITS1 probe revealed a significant accumulation of 45/47S and 41S pre-rRNAs and decreased levels of 30S and 21S pre-rRNAs (Figure 4G). Furthermore, we noted a significant accumulation of 18S-E pre-rRNA in Jazf1-depleted cells, indicating that the last step of 18S rRNA processing was impaired. Similar results were found with the ITS2 probe, revealing an enrichment of 45S and 41S pre-rRNAs but not the 12S pre-rRNA precursor following knockdown of Jazf1 (Figures 4G–4I). Importantly, we found a similar defect in rRNA processing in islets of $Lepr^{db/db}$ mice compared with $Lepr^{+/?}$ islets (Figure 4J), suggesting that rRNA processing may be impaired in T2D. In order to determine the impact of this alteration at the level of the ribosome, we performed a polysome profiling analysis in MIN6 cells in which Jazf1 levels were reduced by RNAi. JAZF1-depleted cells exhibited a lower abundance of free 40S subunits, which contains mature 18S rRNA, and a consequent decrease of 80S ribosomes and polysomes compared with control siRNA-transfected cells (Figure 4K). As alterations in ribosome biogenesis are often associated with changes in the morphology of nucleoli (Mélèse and Xue 1995; Boulon et al., 2010), we stained cells with anti-fibrillarin, a nucleolar protein involved in pre-rRNA processing, to monitor the nucleolus size. Silencing of Jazf1 resulted in larger nucleoli, as determined by an increased ratio between nucleolar and nuclear areas, suggesting a direct correlation between nucleolar size and rRNA processing upon Jazf1 knockdown (Figures 4L and 4M). Collectively, these results indicate that JAZF1 plays an important role in pre-rRNA processing by facilitating the formation of 18S rRNA and ribosomal 40S subunits and thereby regulating protein synthesis.

JAZF1 Regulates the Expression of rRNA Processing and Ribosomal Protein Genes and Influences p53-Dependent Stress Responses

To identify the genes that could mediate the defect in rRNA processing, we queried RNA-seq data from *βJazf1KO* and *βWt* mice for expression changes in transcripts encoding ribosome biogenesis factors. We found significantly dysregulated genes that are involved in rRNA processing (Figure 5A). We examined two factors, respectively, that are upregulated (Tsr3, Nop56) and downregulated (Nol4, UTP14C) in islets of *βJazf1KO* mice. Silencing of Nol4 and UTP14C in MIN6 cells had no effect on rRNA processing (Figure S5A). Tsr3 overexpression led to abnormal 18S rRNA processing compared with control cells (mCherry) when probed with ITS1 (Figures 5B and S5B). Similar defects in pre-rRNA processing were found when we overexpressed Nop56 in MIN6 cells (Figure 5C). Tsr3 catalyzes the base modification of 18S rRNA (Meyer et al., 2016), whereas Nop56 is a component of the box C/D small nucleolar ribonucleoprotein complexes that direct 2-prime-O-methylation of pre-rRNAs during its maturation and therefore may function in an early to middle step of pre-rRNA processing (Hayano et al., 2003). Whereas we did not detect an enrichment of JAZF1 at the *Tsr3* promoter, our ChIP analysis revealed that JAZF1 binds to the promoter region of *Nop56* (Figure 5D).

Defects of rRNA modifications or processing enzymes often lead to disturbed ribosome biogenesis or assembly (King et al., 2003; Liang et al., 2009). This in turn can activate cellular stress responses, including activation of the p53 pathway, a process

(E) Schematic illustration of pre-rRNA processing. Cleavage sites to remove external and internal spacers (ETS/*ITS1/2*) are indicated.
(F–H) Northern blot analysis of MIN6 cells transfected with si-Jazf1 and control siRNAs and hybridized with ETS (F), ITS1 (G), or ITS2 (H) probes.
(I) Densitometric analysis of the pre-rRNA of 18S (ITS1 probe) and 28S (ITS2 probe) of MIN6 cells transfected with si-Jazf1 and control siRNAs (n = 4).
(J) Northern blot analysis of isolated islets from $Lepr^{db/db}$ and wild-type mice, hybridized with the indicated probes.
(K) Polysome profiling analysis of MIN6 cells transfected with si-Jazf1 and control siRNAs.
(L and M) Immunohistochemical staining of nucleolar protein fibrillarin and DNA (DAPI) in MIN6 cells transfected with si-Jazf1 and control si-RNAs (L) and quantification of stained fibrillarin/DAPI area (M). Scale bar: 10 μm (n = 3).
Data are presented as mean ± SD; *$p \leq 0.05$, **$p \leq 0.01$, ***$p \leq 0.001$, and ****$p \leq 0.0001$ by two-way ANOVA (Sidak's multiple-comparison test) (I) or Student's t test (A–D and M).

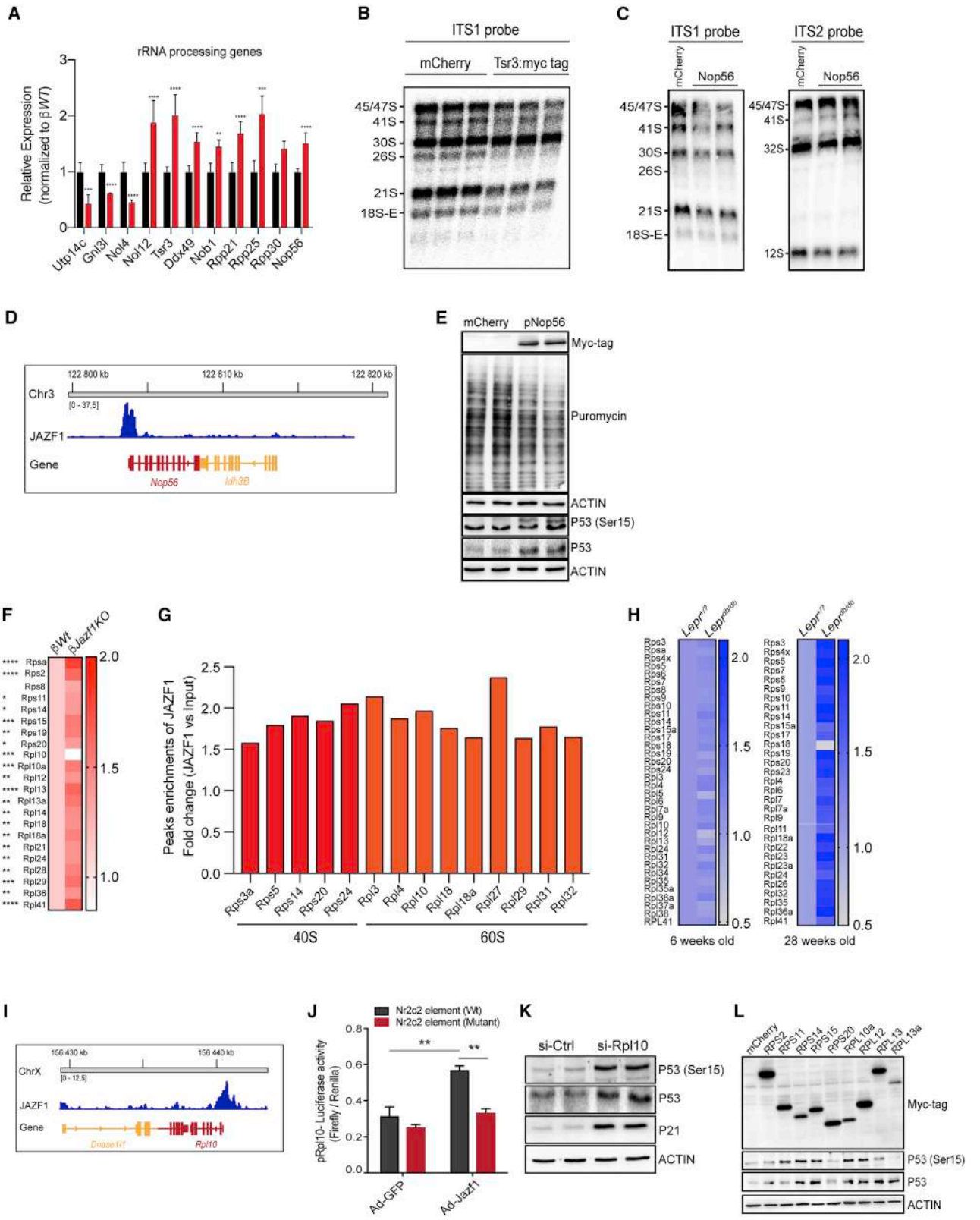

(legend on next page)

named "ribosomal stress" (Boulon et al., 2010; Wang et al., 2015). We elicited ribosomal stress by treating MIN6 cells with low doses of actinomycin D, known to selectively inhibit RNA polymerase I (Perry and Kelley, 1970), which resulted in decreased protein translation and a strong activation of p53 and apoptosis (Figure S5C). Interestingly, increased Nop56 expression was sufficient to impair protein translation and activate p53 and its target p21 (Figure 5E), whereas Tsr3 overexpression had no effect on protein translation but was sufficient to activate p53 (Figures S5D and S5E). These data show that JAZF1 directly and indirectly regulates rRNA biogenesis factors that alter pre-rRNA processing and stimulate ribosomal stress responses.

Our transcriptomic analysis in *βJazf1KO* mice revealed increased levels of several 40S and 60S ribosomal protein (RP) genes compared with *βWt* mice (Figure 5F). In line with the RNA-seq data, ChIP-seq analysis showed that JAZF1 binds to the promoters of five small (40S) and nine large (60S) RP genes (Figure 5G). Interestingly, the levels of RPs are not affected in islets of prediabetic $Lepr^{db/db}$ mice, when Jazf1 expression is unchanged, but in older diabetic $Lepr^{db/db}$ mice, when Jazf1 expression was reduced by 50%, RPs were significantly increased compared with WT controls (Figures 1C and 5H). These findings are consistent with recent studies showing increased expression of RP genes in islets from $Lepr^{db/db}$ mice (El Ouaamari et al., 2015).

We next studied the transcriptional regulation of selected JAZF1-targeted RPs by perturbing JAZF1 levels using luciferase reporter assays. We first confirmed the reduced levels of Rpl10 in islets of *βJazf1KO* mice (Figure S5F) and found that overexpression of JAZF1 resulted in increased Rpl10 promoter activity. This regulation was dependent on an intact Nr2c2 element in the promoter of Rpl10 and supports the negative regulation of JAZF1 on this promoter (Figures 5I and 5J). Conversely, the Rps14, which is also a direct JAZF1 target and overexpressed in islets of *βJazf1KO* mice (Figures 5F and S5G), showed decreased transcript levels when Jazf1 was overexpressed and increased expression upon silencing of Jazf1 (Figure S5H), which corroborates the upregulation in islets of diabetic $Lepr^{db/db}$ mice (Figure 5H). This JAZF1 transcriptional control was also dependent on an Nr2c2 element in the Rps14 promoter (Figure S5I).

The observed ribosome defects in *βJazf1KO* mice led us to hypothesize that the "disturbance" of ribosome subunit components induces an "imbalance state" in the cell, activating the p53 pathway and consequently cell-cycle arrest, thereby influencing proliferation and apoptosis (Zhang and Lu, 2009; Warner and McIntosh, 2009). To explore if the silencing of Rpl10 and overexpression of various RPs in *βJazf1KO* islets can activate the p53 pathway, we knocked down Rpl10 and overexpressed RPs of the small and large subunit in INS1E cells. Both silencing of Rpl10 and overexpression of Rps-11, Rps-14, Rps-15, Rpl10a, and Rpl12 activated the p53 pathway (Figures 5K and 5L). These findings indicate that JAZF1 is required for tight control of rRNA processing and RP transcription and for the coordination of these processes with cell survival pathways.

JAZF1 Regulates Aminoacyl-tRNA Synthetases

Our ChIP-seq analysis demonstrated that JAZF1 binds to the promoters of seven aminoacyl-tRNA synthetase genes (aaRSs) (Figure 6A), consistent with the KEGG analysis of JAZF1 target genes revealing that "aaRSs" ranked second in the enrichment gene sets after "ribosome" (Figure S3D). aaRSs are composed of 20 different ligases that catalyze the ligation of a specific amino acid to its cognate tRNA, thereby ensuring the fidelity of protein synthesis (Ibba and Söll, 2000). The expression levels of two aaRSs, aspartyl-tRNA synthetase (Dars) and glycyl-tRNA synthetase (Gars), were decreased in islets from *βJazf1KO* compared with *βWt* mice (Figure 6B) and JAZF1 was found in ChIP studies to bind to their respective promoter regions (Figures 6C and 6D). Moreover, silencing of Jazf1 in INS1E cells resulted in lower mRNA levels of Gars and Dars compared with si-control-transfected cells (Figure 6E). Adenoviral overexpression of Jazf1 elicited the opposite transcriptional regulation of Dars and Gars compared with Ad-GFP-infected cells (Figure 6F). Furthermore, transcript levels of Dars and Gars were significantly decreased in islets of diabetic $Lepr^{db/db}$ mice (Figure 6G). Of note, in humans, the mRNA levels of Gars are the most highly expressed in pancreas compared with other tissues (Antonellis et al., 2003) and further enriched in β-cells (Park et al., 2010). To investigate if reduced expression of Dars and Gars can be linked to ER stress and activation of cell death pathways, we silenced these aaRSs in the presence and absence of ER stress.

Figure 5. JAZF1 Regulates rRNA Processing and Ribosomal Protein Transcription

(A) Expression levels of pre-rRNA processing genes in islets of *βJazf1KO* and *βWt* control mice (n = 3).

(B and C) Northern blot analysis of MIN6 cells transfected with expression plasmids for Tsr3 (B) and Nop56 (C) and hybridized with indicated probes. mCherry plasmid was used as a control.

(D) Genome Browser tracks of ChIP-seq peaks in INS1E cells. Region spanning the Nop56/Idh3B genes on chromosome 3 is shown. ChIP-seq peaks are presented after normalizing to input.

(E) Western blot analysis of indicated proteins in MIN6 cells transfected with Nop56 and control (mCherry) expression plasmids. Protein synthesis was assessed using puromycin labeling.

(F) Heatmap of ribosomal gene expression in islets of *βJazf1KO* and *βWt* mice.

(G) Peak enrichment of JAZF1 on promoters of indicated ribosomal proteins of 40S and 60S subunits in INS1E cells.

(H) Heatmap of relative ribosomal gene expression in islets of $Lepr^{db/db}$ and control mice at 6 and 28 weeks of age.

(I) Genome Browser tracks of ChIP-seq peaks in INS1E cells. Region spanning the Dnase1l1/Rpl10 genes on the X chromosome is shown.

(J) Luciferase reporter assay of INS1E cells transfected with plasmids containing wild-type (WT) Rpl10 promoter or a mutated Nr2c2 site (mutant) and infected with either a control or Jazf1-expressing adenovirus (Ad-Jazf1). Levels are relative to Renilla luciferase activity (n = 5).

(K and L) Western blot analysis of indicated proteins in INS1E cells transfected with si-Rpl10 or control siRNAs (K) or expression plasmids of indicated myc-tagged ribosomal genes (L).

Data are presented as mean ± SD; *$p \leq 0.05$, **$p \leq 0.01$, ***$p \leq 0.001$, and ****$p \leq 0.0001$ by two-way ANOVA (Sidak's multiple-comparison test) (J) or Student's t test (A).

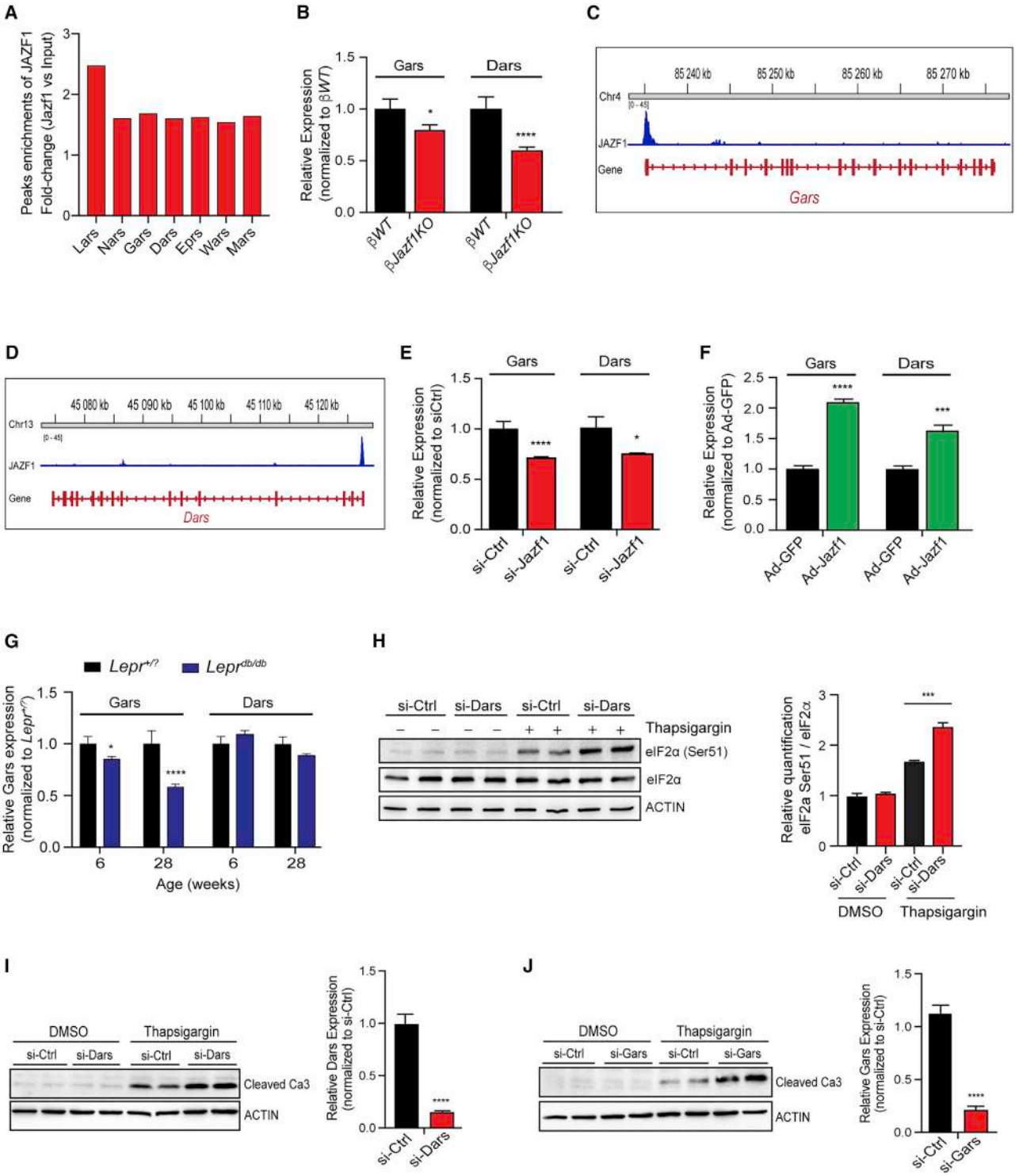

Figure 6. JAZF1 Regulates the Expression of Aminoacyl-tRNA Synthetase Genes

(A) Peak enrichment of JAZF1 in ChIP-seq analysis of INS1E cells on promoters of indicated aminoacyl-tRNA synthetase genes.

(B) Relative expression levels of Gars and Dars in islets of *βJazf1KO* and *βWt* control mice (n = 3).

(C and D) Genome Browser tracks of ChIP-seq peaks in INS1E cells. Regions spanning the Gars (C) and Dars (D) genes, respectively, are shown. ChIP-seq peaks were normalized to input.

(legend continued on next page)

No evidence for ER stress was observed upon Gars knockdown, but we measured increased phosphorylation of eIF2α when Dars was silenced (Figure 6H). This finding underlines recent reports suggesting that deficiency states of aaRSs are linked to the ER stress response (Krokowski et al., 2013; Fröhlich et al., 2017). Moreover, knockdown of Dars and Gars rendered the susceptibility to apoptosis upon exposure to ER stress (Figures 6I and 6J). Together, these findings show that JAZF1 is a positive and direct transcriptional regulator of aaRSs, which play a crucial role in translation and ER stress-mediated apoptosis of pancreatic β-cells.

Srp54a and Insulin Are Direct Targets of JAZF1

SRP54a is a key component of the ribonucleoprotein complex that interacts with ribosomes to bring the translocation of secretory and membrane proteins to the ER (Focia et al., 2004). We noted that Srp54a transcript levels were 2-fold lower in islets of *βJazf1KO* mice compared with controls (Figure 7A). Our ChIP-seq data further demonstrated that JAZF1 binds to the Srp54a promoter region (Figure 7B). Recently, it has been shown that mutations in *SRP54a* cause Shwachman-Bodian-Diamond syndrome, a recessive disease characterized by exocrine pancreatic insufficiency, bone marrow failure, and skeletal dysplasia, but may also present with early infancy diabetes (Kamoda et al., 2005). Loss-of-function mutations and knockdown of *SRP54a* have been shown to induce ER stress and are associated with apoptosis in human bone marrow cells (Bellanné-Chantelot et al., 2018). Interestingly, we found that Srp54a levels are increased and reduced in islets from prediabetic and diabetic $Lepr^{db/db}$ mice, respectively, compared with control mice (Figure 7C). Moreover, knockdown of Srp54a in INS1E cells induced the phosphorylation of eIF2α and increased levels of cleaved caspase-3 (Figure 7D). These data indicate that JAZF1 participates in the regulation of SRP54a expression, which plays a crucial role in ER stress-mediated apoptosis of β-cells.

Our ChIP-seq data also identified enriched binding of JAZF1 at the proximal promoter region of the *Ins1* gene (Figure 7E). Furthermore, the NHR scan analysis identified a direct repeat (DR1) Nr2c2 element located at −61 to −49 bp relative to the TSS and contained the consensus hexanucleotide sequence AGGTCA. Importantly, this element is conserved among mouse, rat, and human genomes (Figure S6A). In the human promoter, it is located between nucleotide positions −276 and −264 bp relative to the TSS. Of note, this motif is located in the previously described glucose-responsive element (Z element) (−292 to −243 bp) that acts both as a glucose-responsive enhancer in primary cultured islet cells and as a transcriptional repressor in immortalized β- and non-β-cells (Sander et al., 1998; Pino et al., 2005).

Our RNA-seq and qPCR analysis revealed that the transcript levels of *Ins1* were increased in islets of *βJazf1KO* compared with *βWt* mice, whereas Ins2 mRNA levels were unchanged (Figure 7F). In addition, INS1E cells infected with a Jazf1-expressing adenovirus had reduced levels of Ins1 compared with cells infected with a control virus (Figures 7G and 7H). Overexpression of Jazf1 in dispersed human islet cells resulted in decreased *INS* transcript levels compared with control (Ad-GFP) infected cells (Figure 7I), indicating that the transcriptional regulation of the *INS* gene by JAZF1 is conserved between rodents and human.

To determine if JAZF1 regulates human insulin gene transcription through the NR2C2 DR1 element, we generated three luciferase reporters with upstream human insulin promoter sequences (WT), or identical constructs harboring point mutations (mutant), or a deletion of the NR2C2 DR1 motif (Figure 7J). These reporter constructs were transfected into EndoC-βH2 human cells in which JAZF1 was either present or silenced by RNAi. The basal activity of the human insulin promoter was increased in Jazf1-depleted cells. Remarkably, this activation was abolished in reporter plasmids harboring a NR2C2 mutant or deletion element (Figure 7K), indicating that the DR1 element is required for the regulation of the human insulin gene by JAZF1. Of note, *βJazf1KO* mice exhibited higher levels of serum proinsulin compared with *βWt* animals, an observation that is in agreement with the higher proinsulin levels found in human and rodent T2D. These results demonstrate key roles for JAZF1 in protein translation by transcriptional regulation of Srp54a, a protein that links three key elements of the SRP complex (i.e., the 7SL RNA, the signal sequence of the nascent ribosome-bound polypeptide chain, and the signal peptide receptor on the ER membrane), as well as the insulin gene through a conserved negative regulatory element (NRE) containing a DR1 site in the *INS* promoter, whose mechanistic basis of repression has remained elusive.

DISCUSSION

In this study we confirm in a large cohort that the SNP rs1635852, located in intron X of *JAZF1*, is a T2D susceptibility gene. Rs1635852 is located in a key region of a β-cell enhancer and mediates allele-specific differences in JAZF1 expression, with the T2D risk allele T exhibiting lower transcriptional activity than the nonrisk allele C. Furthermore, the risk allele also mediates increased binding to protein complexes involving JAZF1, suggesting that it functions as part of a transcriptional repressor complex (Fogarty et al., 2013). Our study also demonstrates that JAZF1 is a key factor in pancreatic β-cells for sensing metabolic stress signals and for mediating a dynamic and coordinated transcriptional response that regulates protein translation in response to increased insulin demand. JAZF1 is enriched in β-cells and dynamically distributed in the cytoplasm and nucleus, with a predominantly cytosolic localization with low glucose in mice and healthy human subjects and a nuclear presence upon stimulation with high glucose and in different murine models (*Akita*, *db/db*) and in pancreatic sections of patients with

(E–G) Expression levels of Gars and Dars in INS1E cells upon silencing using siRNAs (E) or overexpression of Jazf1 (Ad-Jazf1) compared with control cells (Ad-GFP) (F) and in islets of $Lepr^{db/db}$ and control mice ($Lepr^{+/?}$) at 6 and 28 weeks of age (G). n = 3 per group.
(H–J) Western blot analysis of eIF2α (Ser51), eIF2α (H) and cleaved caspase-3 (I and J) in INS1E cells following transfection of siRNAs targeting Dars (H and I) or Gars (J) in response to thapsigargin (TG) for 5 h. Quantification of band intensities by densitometry are shown on right. All data are in duplicates.
Data are presented as mean ± SD; *p ≤ 0.05, **p ≤ 0.01, ***p ≤ 0.001, and ****p ≤ 0.0001 by Student's t test.

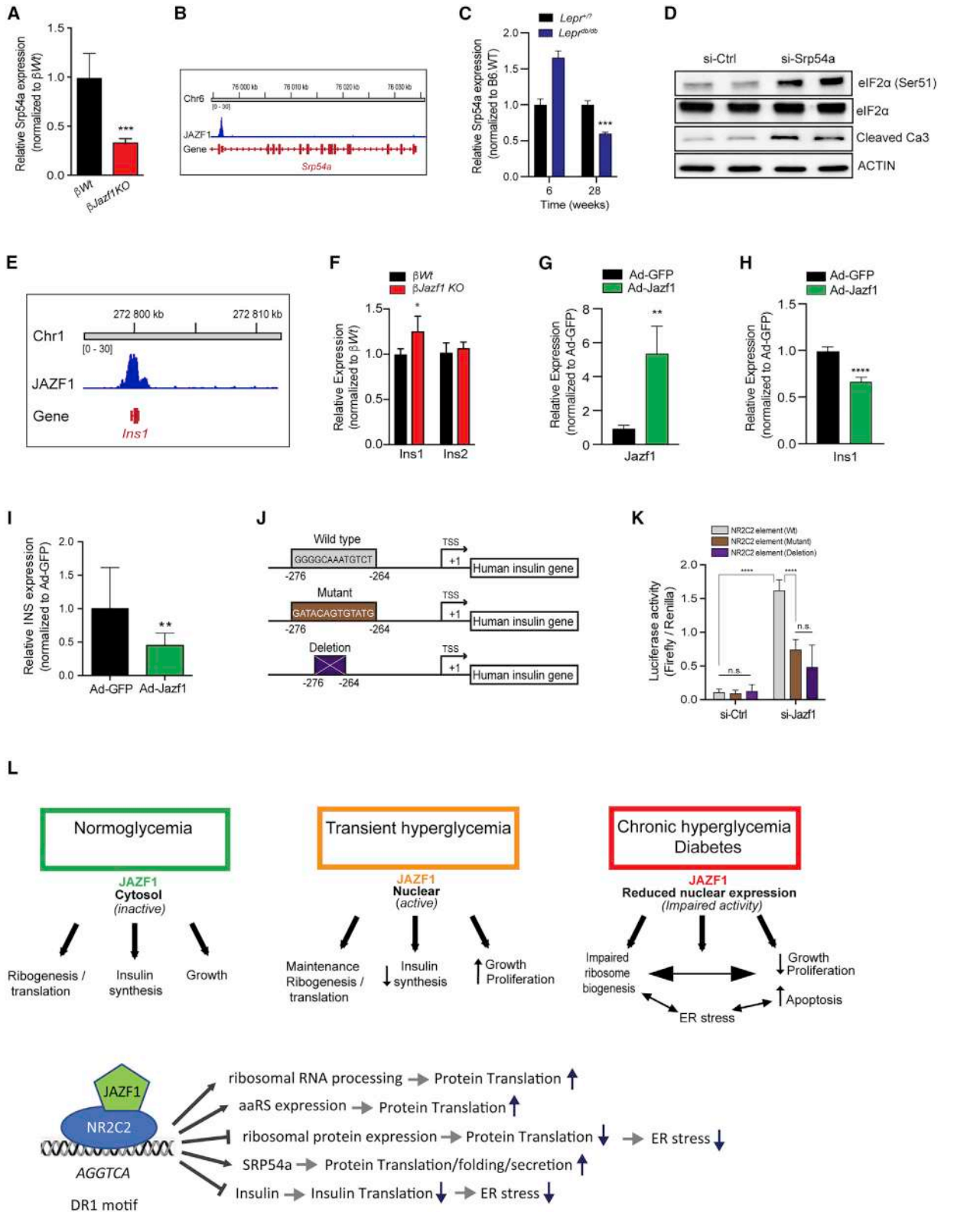

(legend on next page)

T2D. Although our mouse genetic studies show that JAZF1 is dispensable for normal β-cell function, it is clear that during increased insulin demand or β-cell growth, JAZF1 translocates to the nucleus, thereby influencing the transcription and the expression of its target genes. The mechanisms by which JAZF1 translocates to the nucleus during metabolic stress may be mediated by increased Ca^{2+} levels, induced by high glucose and/or cytokine signaling, or by a calcineurin-mediated process that dephosphorylates JAZF1, thereby exposing nuclear import signals leading to translocation in the nucleus, where Jazf1 regulates transcription (Cartwright and Helin, 2000). This model is supported by several conserved phosphorylated serine and tyrosine residues in JAZF1. It will be important to determine the kinases and phosphatases that regulate stress- and glucose-mediated nuclear import in pancreatic β-cells. We show that in diabetic states, the nuclear shuttling of JAZF1 in β-cells is intact, but the overall expression levels are significantly reduced in diabetic rodents, in islets of T2D patients, and in islets exposed to chronic metabolic stress, findings that support a study reporting reduced JAZF1 levels in human islets of hyperglycemic donors (Taneera et al., 2012). These results indicate that in chronic stress conditions, JAZF1 function is impaired, contributing to progressive β-cell dysfunction as shown in *Akita βJazf1KO* mice that have a markedly accelerated disease progression due to increased β-cell apoptosis and decreased proliferation (Figure 7L).

Our analysis of ChIP-seq and RNA-seq revealed that JAZF1 is a transcriptional mediator of ribosome biogenesis, including 40S and 60S subunit genes, rRNA processing, and aaRSs, and that these processes are impaired in murine T2D (Figure 7L). These findings are consistent with RNA-seq analysis from islets of human T2D showing ribosome biogenesis transcripts as the most enriched gene set (De Jesus et al., 2019; Li et al., 2018). Our data are also consistent with JAZF1 being an ortholog of yeast Sfp1, a master transcriptional regulator of ribosome biogenesis in yeast (De Virgilio and Loewith, 2006).

Our morphometric analysis of nucleoli revealed that their size is enlarged in Jazf1-depleted β-cells, and their shape remained intact. This appearance resembles what has been seen in aging cell culture models and in senescent cells (BeMiller and Lee, 1978; Bowmann et al., 1976). Conversely, small nucleoli are a cellular hallmark of longevity in mutant as well as calorie-restricted organisms, which also exhibit decreased expression of ribosomal RNA and proteins, including fibrillarin (Tiku et al., 2017). Recent evidence suggests additional roles for nucleoli as key hubs for sensing and reacting to various stress stimuli such as induction of senescence, DNA damage by activating the p53 pathways, cell-cycle arrest, and apoptosis (Deisenroth et al., 2016). Furthermore, nucleolar stress and p53 activation, both present in islets of diabetic *βJazf1KO* mice, have also been associated with increased nucleoli size (James et al., 2014). The increased nucleolar size in β-cells that are depleted in JAZF1 are therefore consistent with these published reports but may be attributed to the increased synthesis of RP, as ~1/3 of all nucleolar proteins detected by mass spectrometry are composed of RPs (Boisvert et al., 2007; Lam et al., 2010).

One of the most striking results of our study is the finding that in response to experimental conditions of ER stress, Jazf1 transcripts and nuclear protein levels are reduced, leading to increased ER stress and susceptibility to apoptosis. Data from mutant *Jazf1* mice also show that JAZF1 contributes to ER homeostasis. Previous studies have shown that increased protein synthesis can lead to upregulation of the UPR pathway through accumulation of misfolded proteins (Harding et al., 2000a, 2000b; Ron, 2002). We found that deletion of *Jazf1* induces the expression of UPR-related genes, whereas Jazf1 overexpression elicits the opposite transcriptional response. We implicate three processes in leading to the activation of ER stress in the absence of JAZF1: impaired rRNA processing, abnormal RP expression, and defective transcriptional regulation of tRNAs. The observed defect in rRNA processing upon in *βJazf1KO* mice can be predicted to affect ribosome assembly and protein production. Moreover, we uncover a previously unrecognized defect in rRNA processing and translation in islets from *db/db* mice at the decompensation stage. Our RNA-seq and ChIP-seq analysis further indicate that the gene encoding Nop56, which is a direct JAZF1 target, is responsible for the impairment in rRNA processing, as overexpression of Nop56 in β-cells led to

Figure 7. JAZF1 Is a Transcriptional Regulator of the *SRP54a* and *INS* Genes

(A) Srp54a transcript levels of *βJazf1KO* and *βWt* control mice. n = 3 per group.

(B) Genome Browser tracks of ChIP-seq peaks in INS1E cells. Region spanning the *Srp54a* gene and its promoter is shown. ChIP-seq peaks are presented after normalizing to input.

(C) Expression of Srp54a in islets of 6- and 28-week-old $Lepr^{db/db}$ and wild-type control mice.

(D) Western blot of indicated proteins in INS1E cells following transfection with si-Srp54a or si-Ctrl. Actin was used as a loading control.

(E) Genome Browser tracks of ChIP-seq peaks in INS1E cells. Approximately 20 kb region spanning the murine Ins1 locus is shown on chromosome 1. ChIP-seq peaks are presented after normalizing to input.

(F) Relative expression levels of *Ins1* and *Ins2* in islets of *βJazf1KO* and *βWt* mice.

(G–I) Relative expression of Jazf1 (G) and Ins1 (H) in INS1E cells, and INS (I) in dispersed human islets following Ad-Jazf1 or control Ad-GFP infection. n = 3 per group.

(J) Schematic representation of reporter plasmids harboring the human insulin promoter with wild-type, mutant, or a deleted DR1 element site. TSS, transcription start site.

(K) Luciferase activity assays in Endoc-βH2 cells transfected with firefly luciferase reporter constructs shown in (J). Data are normalized to Renilla luciferase. n = 5 for each group.

(L) Illustration of model depicting the role of JAZF1 in normal (green) conditions and in response to short (orange) and chronic (red) exposure to metabolic stress. Bottom: illustration of model showing the molecular function of JAZF1 in active (nuclear) conditions.

Data are presented as mean ± SD; *$p \leq 0.05$, **$p \leq 0.01$, ***$p \leq 0.001$, and ****$p \leq 0.0001$ by two-way ANOVA (Sidak's multiple-comparison test) (K) or Student's t test (A, C, and F–I).

defect in 18S and 28S processing. This finding is in line with a recent study demonstrating that knockdown or overexpression of Nop56 results in defects in pre-rRNA processing (Lykke-Andersen et al., 2018).

We also discovered that JAZF1 is a prominent regulator of numerous RPs and demonstrate that JAZF1 is responsible for maintaining the balance between the components of ribosomal subunits (rRNA and RPs) for optimal ribosome synthesis. Ablation of *Jazf1* in islets revealed increased levels of many RP transcripts, accompanied by a reduction in the 40S subunit, indicating that JAZF1 is primarily a negative transcriptional regulator of RPs. Our data therefore offer a mechanistic explanation for a recent study reporting increased levels of subsets of RPs in a rat T2D model compared with control islets using unbiased quantitative proteomic analysis (Hou et al., 2017). An emerging body of literature suggests that rRNA processing and ribosome biogenesis are tightly orchestrated processes and that imbalances in synthesis or turnover can affect signaling pathways and disease development. Furthermore, these pathways are linked to p53 activation as a general response to defective ribosome function (Barlow et al., 2010; Dutt et al., 2011). For example, Rps6 haploinsufficiency activates the p53 pathway in mouse embryonic cells and T lymphocyte cells (Sulic et al., 2005). Zebrafish with a heterozygous Rpl11 mutation exhibit increased glucose levels and upregulated preproinsulin transcript level (Danilova et al., 2011). Furthermore, conditional inactivation of Rps14 in mice leads to a p53-dependent erythroid differentiation defect (Schneider et al., 2016). Interestingly, overexpression or silencing of single RPs is sufficient to affect ribosome biogenesis and induce activation of the p53 pathway (Lohrum et al., 2003; Zhou et al., 2013). We show that silencing or overexpression of the JAZF1 targets Rpl10 and Rps14 is sufficient to perturb protein synthesis and induce p53 activation and apoptosis. Of note, GWASs have identified an association between p53 and T2D susceptibility (Gaulton et al., 2008; Burgdorf et al., 2011), which is consistent with our and other studies showing evidence of DNA damage and p53 activation in islets of *db/db* mice and human T2D subjects (Tornovsky-Babeay et al., 2014; Belgardt et al., 2015). Together, our study describes a previously unrecognized mechanism in T2D in which defective ribosome synthesis during metabolic stress activates p53 and apoptosis in β-cells.

In this study, we show that JAZF1 is a direct transcriptional activator of genes encoding aminoacyl tRNA synthetases. Mutations in tRNA ligases frequently give rise to diseases with neuronal pathologies and autoimmune and metabolic disorders. Specifically, mutations in glycine tRNA ligase (GARS) are associated with childhood neuropathological diseases alongside altered mitochondrial protein and respiratory chain subunit expression (Boczonadi et al., 2018). Our finding that GARS levels are reduced by 50% in *db/db* mice and that silencing of Gars and Dars renders β-cells more sensitive to ER stress-mediated apoptosis corroborates phenotypic traits in mice with mutated tRNA synthetase exhibiting impaired translational fidelity, protein misfolding, and induction of ER stress (Lee et al., 2006).

Our study demonstrates that JAZF1 is a direct transcriptional activator of Srp54a, a component of the signal recognition particle complex that is recognized by the signal sequence of the nascent polypeptide on the ribosome and docked to the ER membrane via the conjugate receptors. In β-cells, Srp54a binds to the preproinsulin signal sequence appearing from the ribosome and slows down protein synthesis, which can prevent the premature initiation of preproinsulin folding prior to nascent peptide to the ER membrane (Eskridge and Shields, 1983; Walter and Blobel, 1983). We show that deletion of Srp54a leads to increased phosphorylated eIF2α levels and induces apoptosis. Importantly, Srp54a levels were decreased in absence of JAZF1; furthermore, Srp54a expression was reduced in islets of *db/db* mice where chronic ER stress is induced. Interestingly, five mutations located in the preproinsulin signal peptide have been reported to cause diabetes in humans (Støy et al., 2007; Garin et al., 2010). Collectively, we propose that under chronic insulin demand, in conditions of partial or absolute JAZF1 deficiency, JAZF1 contributes to ER stress through increasing insulin transcription directly and through defective expression of Srp54, which can lead to cytosolically misassembled, misfolded, and mislocalized proteins (Bellanné-Chantelot et al., 2018).

Insulin is a major ER client protein in β-cells, and high levels of misfolded insulin protein can affect the protein folding capacity and elicit ER stress. Interestingly, the serum proinsulin level and proinsulin/insulin ratio were higher in *Akita βJazf1KO* mice compared with *Akita βWt* mice. Previously, it has been shown that the proinsulin/insulin ratio is increased in *Akita* mice, which exhibit high levels of ER stress in β-cells (Winnay et al., 2014). This observation is consistent with elevated proinsulin/insulin ratios in human T2D (Ward et al., 1987; Vangipurapu et al., 2015) and with studies demonstrating that proinsulin misfolding is an early feature in the progression of prediabetes (Liu et al., 2005; Arunagiri et al., 2019). Furthermore, transgenic insulin-overexpressing mice exhibit glucose intolerance in the absence of obesity (Shanik et al., 2008), and insulin-knockout mice are partially protected from chronic ER stress in β-cells (Szabat et al., 2016). These data indicate that JAZF1 can alleviate ER stress by reducing insulin synthesis, a notion that is supported by the phenotype of transgenic Jazf1 mice that have reduced fasting plasma insulin levels and enhanced glucose tolerance (Yuan et al., 2015).

In this context and on the basis of our gene expression analysis from mutant JAZF1 in human and rodent islets and further supported by the JAZF1 ChIP-seq analysis, it is relevant that we also found the insulin promoter to be a direct JAZF1 target. JAZF1 binds to a conserved DR1 site in the *Ins1* promoter, which is absent in Ins2 due to a nucleotide substitution. These observations are consistent with the transcriptional regulation of *Ins1* but not *Ins2*. Interestingly, in humans, we identified a DR1 site in the insulin promoter within a previously described inhibitory sequence (−279 to −258), also referred to as the NRE (Boam et al., 1990; Clark et al., 1995). This element also lies within the glucose-sensing Z element (−243 to −292) (Sander et al., 1998; Pino et al., 2005), which functions as an enhancer in primary islet cells but represses transcription in immortalized β-cells. Furthermore, the direct regulation of the insulin gene by JAZF1 might contribute to the low insulin content of transformed β-cell lines and act as a protective mechanism to counteract glucose toxicity by downregulating insulin secretion

during chronic hyperglycemia and thereby relieving ER stress and facilitating cell survival.

In summary, our study reveals JAZF1 as an important regulator of ER stress and ribosome biogenesis via a feedback action preventing the activation of ER and p53 stress-mediated β-cell apoptosis. These findings further highlight the crucial influence of JAZF1 on β-cell function. Finally, modulating JAZF1 activity may be a potential pharmacological strategy to alleviate β-cell stress and promote β-cell survival in T2D.

STAR★METHODS

Detailed methods are provided in the online version of this paper and include the following:

- KEY RESOURCES TABLE
- RESOURCE AVAILABILITY
  - Lead Contact
  - Materials Availability
  - Data and Code Availability
- EXPERIMENTAL MODEL AND SUBJECT DETAILS
  - Mouse models
  - Generation of βJazf1KO mice
  - Animal procedures
  - Blood glucose measurements IPGTT and BrdU injection
  - Cell culture and transfections
  - MIN6
  - EndoC-βH2:
  - Expression and purification of recombinant Zinc finger domains
  - Antibody production
  - Recombinant adenoviruses
  - Human islets and pancreatic sections
  - Mouse pancreatic islet
- METHOD DETAILS
  - Immunohistochemistry and β-cell mass measurements
  - Insulin and Proinsulin
  - Dispersed islets experiments
  - Transfections
  - Treatment with reagents
  - Stress induction of human islets with **glucose, palmitate, and cytokines**
  - RNA isolation and quantification
  - Northern blot
  - Luciferase assay
  - Polysome profiling
  - Proteomic studies
  - Immunoblot analysis
  - Cellular fractionation
  - Co-Immunoprecipitation assay
  - Puromycin analysis
  - Illumina RNA sequencing
  - Jazf1 expression in islets from human and mouse T1D model
  - ChIP-Seq assay
  - ChIP-seq data processing
  - Differential binding
  - Functional characterization with GO terms
  - Motif discovery
  - UK BioBank data processing
- QUANTIFICATION AND STATISTICAL ANALYSIS
  - Statistical analysis
- ADDITIONAL RESOURCES

SUPPLEMENTAL INFORMATION

Supplemental Information can be found online at https://doi.org/10.1016/j.celrep.2020.107846.

ACKNOWLEDGMENTS

We wish to thank Hasan Kabakci and Regina Kubsch for excellent technical assistance and Alexandra Title and Mary LaPierre for preparing the manuscript. We thank Functional Genomics Center Zurich for RNA-seq (Lennart Opitz), the Scientific Center for Optical and Electron Microscopy (ScopeM), the Eidgenössische Technische Hochschule (ETH) Flow Cytometry Core Facility (E-FCCF) for support, and F. Quazi for technical contributions in the early stages of the project. This work was supported in part by the Swiss National Research Foundation, Switzerland (M.S.) and the Starr Foundation International (M.S.).

AUTHOR CONTRIBUTIONS

A.K. and M.S. designed the study. A.K. and S.G. performed most of the experiments. A.K. analyzed and interpreted data and wrote the manuscript. E.A. and U.G. provided the UK Biobank analysis. M.W.S. performed the ChIP-seq analysis. The human pancreatic sections of healthy and T2D subjects were made available by G.S. and H.M. M.S. supervised the project and wrote the manuscript. All authors read the manuscript.

DECLARATION OF INTERESTS

The authors declare no competing interests.

Received: January 16, 2020
Revised: April 23, 2020
Accepted: June 11, 2020
Published: July 7, 2020

REFERENCES

Accili, D., Talchai, S.C., Kim-Muller, J.Y., Cinti, F., Ishida, E., Ordelheide, A.M., Kuo, T., Fan, J., and Son, J. (2016). When β-cells fail: lessons from dedifferentiation. Diabetes Obes. Metab. *18* (*Suppl 1*), 117–122.

Albert, B., Tomassetti, S., Gloor, Y., Dilg, D., Mattarocci, S., Kubik, S., Hafner, L., and Shore, D. (2019). Sfp1 regulates transcriptional networks driving cell growth and division through multiple promoter-binding modes. Genes Dev. *33*, 288–293.

Alexa, A., Rahnenführer, J., and Lengauer, T. (2006). Improved scoring of functional groups from gene expression data by decorrelating GO graph structure. Bioinformatics *22*, 1600–1607.

Antonellis, A., Ellsworth, R.E., Sambuughin, N., Puls, I., Abel, A., Lee-Lin, S.Q., Jordanova, A., Kremensky, I., Christodoulou, K., Middleton, L.T., et al. (2003). Glycyl tRNA synthetase mutations in Charcot-Marie-Tooth disease type 2D and distal spinal muscular atrophy type V. Am. J. Hum. Genet. *72*, 1293–1299.

Arunagiri, A., Haataja, L., Cunningham, C.N., Shrestha, N., Tsai, B., Qi, L., Liu, M., and Arvan, P. (2018). Misfolded proinsulin in the endoplasmic reticulum during development of beta cell failure in diabetes. Ann. N Y Acad. Sci. *1418*, 5–19.

Arunagiri, A., Haataja, L., Pottekat, A., Pamenan, F., Kim, S., Zeltser, L.M., Paton, A.W., Paton, J.C., Tsai, B., Itkin-Ansari, P., et al. (2019). Proinsulin misfolding is an early event in the progression to type 2 diabetes. eLife *8*, e44532.

Aszódi, A. (2012). MULTOVL: fast multiple overlaps of genomic regions. Bioinformatics *28*, 3318–3319.

Back, S.H., and Kaufman, R.J. (2012). Endoplasmic reticulum stress and type 2 diabetes. Annu. Rev. Biochem. *81*, 767–793.

Barlow, J.L., Drynan, L.F., Hewett, D.R., Holmes, L.R., Lorenzo-Abalde, S., Lane, A.L., Jolin, H.E., Pannell, R., Middleton, A.J., Wong, S.H., et al. (2010). A p53-dependent mechanism underlies macrocytic anemia in a mouse model of human 5q- syndrome. Nat. Med. *16*, 59–66.

Belgardt, B.F., Ahmed, K., Spranger, M., Latreille, M., Denzler, R., Kondratiuk, N., von Meyenn, F., Villena, F.N., Herrmanns, K., Bosco, D., et al. (2015). The microRNA-200 family regulates pancreatic beta cell survival in type 2 diabetes. Nat. Med. *21*, 619–627.

Bellanné-Chantelot, C., Schmaltz-Panneau, B., Marty, C., Fenneteau, O., Callebaut, I., Clauin, S., Docet, A., Damaj, G.-L., Leblanc, T., Pellier, I., et al. (2018). Mutations in the SRP54 gene cause severe congenital neutropenia as well as Shwachman-Diamond-like syndrome. Blood *132*, 1318–1331.

BeMiller, P.M., and Lee, L.-H. (1978). Nucleolar changes in senescing WI-38 cells. Ageing Dev. *8*, 417–427.

Boam, D.S.W., Clark, A.R., and Docherty, K. (1990). Positive and negative regulation of the human insulin gene by multiple trans-acting factors. J. Biol. Chem. *265*, 8285–8296.

Boczonadi, V., Jennings, M.J., and Horvath, R. (2018). The role of tRNA synthetases in neurological and neuromuscular disorders. FEBS Lett. *592*, 703–717.

Boisvert, F.M., van Koningsbruggen, S., Navascués, J., and Lamond, A.I. (2007). The multifunctional nucleolus. Nat. Rev. Mol. Cell Biol. *8*, 574–585.

Bonnefond, A., Froguel, P., and Vaxillaire, M. (2010). The emerging genetics of type 2 diabetes. Trends Mol. Med. *16*, 407–416.

Bookout, A.L., Jeong, Y., Downes, M., Yu, R.T., Evans, R.M., and Mangelsdorf, D.J. (2006). Anatomical profiling of nuclear receptor expression reveals a hierarchical transcriptional network. Cell *126*, 789–799.

Boulon, S., Westman, B.J., Hutten, S., Boisvert, F.M., and Lamond, A.I. (2010). The nucleolus under stress. Mol. Cell *40*, 216–227.

Bowmann, P.D., Meek, R.L., and Daniel, C.W. (1976). Decreased synthesis of nucleolar RNA in aging human cells in vitro. Exp. Cell Res. *101*, 434–437.

Brunstedt, J., and Chan, S.J. (1982). Direct effect of glucose on the preproinsulin mRNA level in isolated pancreatic islets. Biochem. Biophys. Res. Commun. *106*, 1383–1389.

Burgdorf, K.S., Grarup, N., Justesen, J.M., Harder, M.N., Witte, D.R., Jørgensen, T., Sandbæk, A., Lauritzen, T., Madsbad, S., Hansen, T., and Pedersen, O.; DIAGRAM Consortium (2011). Studies of the association of Arg72Pro of tumor suppressor protein p53 with type 2 diabetes in a combined analysis of 55,521 Europeans. PLoS ONE *6*, e15813.

Bycroft, C., Freeman, C., Petkova, D., Band, G., Elliott, L.T., Sharp, K., Motyer, A., Vukcevic, D., Delaneau, O., O'Connell, J., et al. (2018). The UK Biobank resource with deep phenotyping and genomic data. Nature *562*, 203–209.

Cardozo, A.K., Ortis, F., Storling, J., Feng, Y.M., Rasschaert, J., Tonnesen, M., Van Eylen, F., Mandrup-Poulsen, T., Herchuelz, A., and Eizirik, D.L. (2005). Cytokines downregulate the sarcoendoplasmic reticulum pump Ca2+ ATPase 2b and deplete endoplasmic reticulum Ca2+, leading to induction of endoplasmic reticulum stress in pancreatic β-cells. Diabetes *54*, 452–461.

Carlson, M. (2019). org.Rn.eg.db: genome wide annotation for Rat.http://bioconductor.org/packages/release/data/annotation/html/org.Rn.eg.db.html.

Carrero, J.A., Calderon, B., Towfic, F., Artyomov, M.N., and Unanue, E.R. (2013). Defining the transcriptional and cellular landscape of type 1 diabetes in the NOD mouse. PLoS ONE *8*, e59701.

Cartwright, P., and Helin, K. (2000). Nucleocytoplasmic shuttling of transcription factors. Cell. Mol. Life Sci. *57*, 1193–1206.

Cavaghan, M.K., Ehrmann, D.A., and Polonsky, K.S. (2000). Interactions between insulin resistance and insulin secretion in the development of glucose intolerance. J. Clin. Invest. *106*, 329–333.

Chuang, J.C., Cha, J.Y., Garmey, J.C., Mirmira, R.G., and Repa, J.J. (2008). Research resource: nuclear hormone receptor expression in the endocrine pancreas. Mol. Endocrinol. *22*, 2353–2363.

Clark, A.R., Wilson, M.E., Leibiger, I., Scott, V., and Docherty, K. (1995). A silencer and an adjacent positive element interact to modulate the activity of the human insulin promoter. Eur. J. Biochem. *232*, 627–632.

Danilova, N., Sakamoto, K.M., and Lin, S. (2011). Ribosomal protein L11 mutation in zebrafish leads to haematopoietic and metabolic defects. Br. J. Haematol. *152*, 217–228.

De Jesus, D.F., Zhang, Z., Kahraman, S., Brown, N.K., Chen, M., Hu, J., Gupta, M.K., He, C., and Kulkarni, R.N. (2019). m6A mRNA methylation regulates human β-cell biology in physiological states and in type 2 diabetes. Nat Metab *1*, 765–774.

De Virgilio, C., and Loewith, R. (2006). Cell growth control: little eukaryotes make big contributions. Oncogene *25*, 6392–6415.

Degnan, B.M., Degnan, S.M., Naganuma, T., and Morse, D.E. (1993). The ets multigene family is conserved throughout the Metazoa. Nucleic Acids Res. *21*, 3479–3484.

Deisenroth, C., Franklin, D.A., and Zhang, Y. (2016). The evolution of the ribosomal protein-MDM2-p53 pathway. Cold Spring Harb. Perspect. Med. *6*, a026138.

Dooley, J., Tian, L., Schonefeldt, S., Delghingaro-Augusto, V., Garcia-Perez, J.E., Pasciuto, E., Di Marino, D., Carr, E.J., Oskolkov, N., Lyssenko, V., et al. (2016). Genetic predisposition for beta cell fragility underlies type 1 and type 2 diabetes. Nat. Genet. *48*, 519–527.

Durinck, S., Spellman, P.T., Birney, E., and Huber, W. (2009). Mapping identifiers for the integration of genomic datasets with the R/Bioconductor package biomaRt. Nat. Protoc. *4*, 1184–1191.

Dutt, S., Narla, A., Lin, K., Mullally, A., Abayasekara, N., Megerdichian, C., Wilson, F.H., Currie, T., Khanna-Gupta, A., Berliner, N., et al. (2011). Haploinsufficiency for ribosomal protein genes causes selective activation of p53 in human erythroid progenitor cells. Blood *117*, 2567–2576.

El Ouaamari, A., Zhou, J.Y., Liew, C.W., Shirakawa, J., Dirice, E., Gedeon, N., Kahraman, S., De Jesus, D.F., Bhatt, S., Kim, J.S., et al. (2015). Compensatory islet response to insulin resistance revealed by quantitative proteomics. J. Proteome Res. *14*, 3111–3122.

Eskridge, E.M., and Shields, D. (1983). Cell-free processing and segregation of insulin precursors. J. Biol. Chem. *258*, 11487–11491.

Fingerman, I., Nagaraj, V., Norris, D., and Vershon, A.K. (2003). Sfp1 plays a key role in yeast ribosome biogenesis. Eukaryot. Cell *2*, 1061–1068.

Focia, P.J., Shepotinovskaya, I.V., Seidler, J.A., and Freymann, D.M. (2004). Heterodimeric GTPase core of the SRP targeting complex. Science *303*, 373–377.

Fogarty, M.P., Panhuis, T.M., Vadlamudi, S., Buchkovich, M.L., and Mohlke, K.L. (2013). Allele-specific transcriptional activity at type 2 diabetes-associated single nucleotide polymorphisms in regions of pancreatic islet open chromatin at the JAZF1 locus. Diabetes *62*, 1756–1762.

Fröhlich, D., Suchowerska, A.K., Spencer, Z.H., von Jonquieres, G., Klugmann, C.B., Bongers, A., Delerue, F., Stefen, H., Ittner, L.M., Fath, T., et al. (2017). In vivocharacterization of the aspartyl-tRNA synthetase DARS: homing in on the leukodystrophy HBSL. Neurobiol. Dis. *97* (*Pt A*), 24–35.

Garin, I., Edghill, E.L., Akerman, I., Rubio-Cabezas, O., Rica, I., Locke, J.M., Maestro, M.A., Alshaikh, A., Bundak, R., del Castillo, G., et al.; Neonatal Diabetes International Group (2010). Recessive mutations in the INS gene result in neonatal diabetes through reduced insulin biosynthesis. Proc. Natl. Acad. Sci. U S A *107*, 3105–3110.

Gaulton, K.J., Willer, C.J., Li, Y., Scott, L.J., Conneely, K.N., Jackson, A.U., Duren, W.L., Chines, P.S., Narisu, N., Bonnycastle, L.L., et al. (2008). Comprehensive association study of type 2 diabetes and related quantitative traits with 222 candidate genes. Diabetes *57*, 3136–3144.

Grarup, N., Andersen, G., Krarup, N.T., Albrechtsen, A., Schmitz, O., Jørgensen, T., Borch-Johnsen, K., Hansen, T., and Pedersen, O. (2008). Association testing of novel type 2 diabetes risk alleles in the JAZF1, CDC123/CAMK1D, TSPAN8, THADA, ADAMTS9, and NOTCH2 loci with insulin release, insulin sensitivity, and obesity in a population-based sample of 4,516 glucose-tolerant middle-aged Danes. Diabetes *57*, 2534–2540.

Harding, H.P., Novoa, I., Zhang, Y., Zeng, H., Wek, R., Schapira, M., and Ron, D. (2000a). Regulated translation initiation controls stress-induced gene expression in mammalian cells. Mol. Cell *6*, 1099–1108.

Harding, H.P., Zhang, Y., Bertolotti, A., Zeng, H., and Ron, D. (2000b). Perk is essential for translational regulation and cell survival during the unfolded protein response. Mol. Cell *5*, 897–904.

Hayano, T., Yanagida, M., Yamauchi, Y., Shinkawa, T., Isobe, T., and Takahashi, N. (2003). Proteomic analysis of human Nop56p-associated pre-ribosomal ribonucleoprotein complexes. Possible link between Nop56p and the nucleolar protein treacle responsible for Treacher Collins syndrome. J. Biol. Chem. *278*, 34309–34319.

Heinz, S., Benner, C., Spann, N., Bertolino, E., Lin, Y.C., Laslo, P., Cheng, J.X., Murre, C., Singh, H., and Glass, C.K. (2010). Simple combinations of lineage-determining transcription factors prime cis-regulatory elements required for macrophage and B cell identities. Mol. Cell *38*, 576–589.

Ho, M.M., Yoganathan, P., Chu, K.Y., Karunakaran, S., Johnson, J.D., and Clee, S.M. (2013). Diabetes genes identified by genome-wide association studies are regulated in mice by nutritional factors in metabolically relevant tissues and by glucose concentrations in islets. BMC Genet. *14*, 10.

Hoshino, A., Ariyoshi, M., Okawa, Y., Kaimoto, S., Uchihashi, M., Fukai, K., Iwai-Kanai, E., Ikeda, K., Ueyama, T., Ogata, T., and Matoba, S. (2014). Inhibition of p53 preserves Parkin-mediated mitophagy and pancreatic β-cell function in diabetes. Proc. Natl. Acad. Sci. U S A *111*, 3116–3121.

Hou, J., Li, Z., Zhong, W., Hao, Q., Lei, L., Wang, L., Zhao, D., Xu, P., Zhou, Y., Wang, Y., and Xu, T. (2017). Temporal transcriptomic and proteomic landscapes of deteriorating pancreatic islets in type 2 diabetic rats. Diabetes *66*, 2188–2200.

Hull, R.L., Westermark, G.T., Westermark, P., and Kahn, S.E. (2004). Islet amyloid: a critical entity in the pathogenesis of type 2 diabetes. J. Clin. Endocrinol. Metab. *89*, 3629–3643.

Ibba, M., and Söll, D. (2000). Aminoacyl-tRNA synthesis. Annu. Rev. Biochem. *69*, 617–650.

Itoh, N., and Okamoto, H. (1980). Translational control of proinsulin synthesis by glucose. Nature *283*, 100–102.

James, A., Wang, Y., Raje, H., Rosby, R., and DiMario, P. (2014). Nucleolar stress with and without p53. Nucleus *5*, 402–426.

Kamoda, T., Saito, T., Kinugasa, H., Iwasaki, N., Sumazaki, R., Mouri, Y., Izumi, I., Hirano, T., and Matsui, A. (2005). A case of Shwachman-Diamond syndrome presenting with diabetes from early infancy. Diabetes Care *28*, 1508–1509.

Kang, H.S., Okamoto, K., Kim, Y.S., Takeda, Y., Bortner, C.D., Dang, H., Wada, T., Xie, W., Yang, X.P., Liao, G., and Jetten, A.M. (2011). Nuclear orphan receptor TAK1/TR4-deficient mice are protected against obesity-linked inflammation, hepatic steatosis, and insulin resistance. Diabetes *60*, 177–188.

Keane, K.N., Cruzat, V.F., Carlessi, R., de Bittencourt, P.I.H., Jr., and Newsholme, P. (2015). Molecular events linking oxidative stress and inflammation to insulin resistance and β-cell dysfunction. Oxid. Med. Cell. Longev. *2015*, 181643.

King, T.H., Liu, B., McCully, R.R., and Fournier, M.J. (2003). Ribosome structure and activity are altered in cells lacking snoRNPs that form pseudouridines in the peptidyl transferase center. Mol. Cell *11*, 425–435.

Koontz, J.I., Soreng, A.L., Nucci, M., Kuo, F.C., Pauwels, P., van Den Berghe, H., Dal Cin, P., Fletcher, J.A., and Sklar, J. (2001). Frequent fusion of the JAZF1 and JJAZ1 genes in endometrial stromal tumors. Proc. Natl. Acad. Sci. U S A *98*, 6348–6353.

Krokowski, D., Han, J., Saikia, M., Majumder, M., Yuan, C.L., Guan, B.J., Bevilacqua, E., Bussolati, O., Bröer, S., Arvan, P., et al. (2013). A self-defeating anabolic program leads to β-cell apoptosis in endoplasmic reticulum stress-induced diabetes via regulation of amino acid flux. J. Biol. Chem. *288*, 17202–17213.

Kuleshov, M.V., Jones, M.R., Rouillard, A.D., Fernandez, N.F., Duan, Q., Wang, Z., Koplev, S., Jenkins, S.L., Jagodnik, K.M., Lachmann, A., et al. (2016). Enrichr: a comprehensive gene set enrichment analysis web server 2016 update. Nucleic Acids Res. *44* (*W1*), W90-7.

Lam, Y.W., Evans, V.C., Heesom, K.J., Lamond, A.I., and Matthews, D.A. (2010). Proteomics analysis of the nucleolus in adenovirus-infected cells. Mol. Cell. Proteomics *9*, 117–130.

Langhofer, M., Hopkinson, S.B., and Jones, J.C.R. (1993). The matrix secreted by 804G cells contains laminin-related components that participate in hemidesmosome assembly in vitro. J. Cell Sci. *105*, 753–764.

Langmead, B., and Salzberg, S.L. (2012). Fast gapped-read alignment with Bowtie 2. Nat. Methods *9*, 357–359.

Lee, Y.F., Pan, H.J., Burbach, J.P., Morkin, E., and Chang, C. (1997). Identification of direct repeat 4 as a positive regulatory element for the human TR4 orphan receptor. A modulator for the thyroid hormone target genes. J. Biol. Chem. *272*, 12215–12220.

Lee, J.W., Beebe, K., Nangle, L.A., Jang, J., Longo-Guess, C.M., Cook, S.A., Davisson, M.T., Sundberg, J.P., Schimmel, P., and Ackerman, S.L. (2006). Editing-defective tRNA synthetase causes protein misfolding and neurodegeneration. Nature *443*, 50–55.

Lerner, A.G., Upton, J.P., Praveen, P.V., Ghosh, R., Nakagawa, Y., Igbaria, A., Shen, S., Nguyen, V., Backes, B.J., Heiman, M., et al. (2012). IRE1α induces thioredoxininteracting protein to activate the NLRP3 inflammasome and promote programmed cell death under irremediable ER stress. Cell Metab. *16*, 250–264.

Li, B., and Dewey, C.N. (2011). RSEM: accurate transcript quantification from RNA-Seq data with or without a reference genome. BMC Bioinformatics *12*, 323.

Li, L., Pan, Z., Yang, S., Shan, W., and Yang, Y. (2018). Identification of key gene pathways and coexpression networks of islets in human type 2 diabetes. Diabetes Metab. Syndr. Obes. *11*, 553–563.

Liang, X.H., Liu, Q., and Fournier, M.J. (2009). Loss of rRNA modifications in the decoding center of the ribosome impairs translation and strongly delays pre-rRNA processing. RNA *15*, 1716–1728.

Liao, Y., Smyth, G.K., and Shi, W. (2014). featureCounts: an efficient general purpose program for assigning sequence reads to genomic features. Bioinformatics *30*, 923–930.

Liu, M., Li, Y., Cavener, D., and Arvan, P. (2005). Proinsulin disulfide maturation and misfolding in the endoplasmic reticulum. J. Biol. Chem. *280*, 13209–13212.

Liu, N.C., Lin, W.J., Kim, E., Collins, L.L., Lin, H.Y., Yu, I.C., Sparks, J.D., Chen, L.M., Lee, Y.F., and Chang, C. (2007). Loss of TR4 orphan nuclear receptor reduces phosphoenolpyruvate carboxykinase-mediated gluconeogenesis. Diabetes *56*, 2901–2909.

Lohrum, M.A., Ludwig, R.L., Kubbutat, M.H., Hanlon, M., and Vousden, K.H. (2003). Regulation of HDM2 activity by the ribosomal protein L11. Cancer Cell *3*, 577–587.

Love, M.I., Huber, W., and Anders, S. (2014). Moderated estimation of fold change and dispersion for RNA-seq data with DESeq2. Genome Biol. *15*, 550.

Lykke-Andersen, S., Ardal, B.K., Hollensen, A.K., Damgaard, C.K., and Jensen, T.H. (2018). Box C/D snoRNP Autoregulation by a cis-Acting snoRNA in the NOP56 Pre-mRNA. Mol. Cell *72*, 99–111.e5.

Machanick, P., and Bailey, T.L. (2011). MEME-ChIP: motif analysis of large DNA datasets. Bioinformatics *27*, 1696–1697.

Manolio, T.A. (2010). Genomewide association studies and assessment of the risk of disease. N. Engl. J. Med. *363*, 166–176.

Mastracci, T.L., Turatsinze, J.V., Book, B.K., Restrepo, I.A., Pugia, M.J., Wiebke, E.A., Pescovitz, M.D., Eizirik, D.L., and Mirmira, R.G. (2018). Distinct gene expression pathways in islets from individuals with short- and long-duration type 1 diabetes. Diabetes Obes. Metab. *20*, 1859–1867.

Mélèse, T., and Xue, Z. (1995). The nucleolus: an organelle formed by the act of building a ribosome. Curr. Opin. Cell Biol. *7*, 319–324.

Meng, F., Lin, Y., Yang, M., Li, M., Yang, G., Hao, P., and Li, L. (2018). JAZF1 inhibits adipose tissue macrophages and adipose tissue inflammation in diet-induced diabetic mice. BioMed Res. Int. *2018*, 4507659.

Meyer, B., Wurm, J.P., Sharma, S., Immer, C., Pogoryelov, D., Kötter, P., Lafontaine, D.L.J., Wöhnert, J., and Entian, K.D. (2016). Ribosome biogenesis factor Tsr3 is the aminocarboxypropyl transferase responsible for 18S rRNA hypermodification in yeast and humans. Nucleic Acids Res. *44*, 4304–4316.

Mulder, H. (2017). Transcribing β-cell mitochondria in health and disease. Mol. Metab. *6*, 1040–1051.

Nakajima, T., Fujino, S., Nakanishi, G., Kim, Y.S., and Jetten, A.M. (2004). TIP27: a novel repressor of the nuclear orphan receptor TAK1/TR4. Nucleic Acids Res. *32*, 4194–4204.

O'Geen, H., Lin, Y.H., Xu, X., Echipare, L., Komashko, V.M., He, D., Frietze, S., Tanabe, O., Shi, L., Sartor, M.A., et al. (2010). Genome-wide binding of the orphan nuclear receptor TR4 suggests its general role in fundamental biological processes. BMC Genomics *11*, 689.

Oda, Y., Okada, T., Yoshida, H., Kaufman, R.J., Nagata, K., and Mori, K. (2006). Derlin-2 and Derlin-3 are regulated by the mammalian unfolded protein response and are required for ER-associated degradation. J. Cell Biol. *172*, 383–393.

Oikawa, T., and Yamada, T. (2003). Molecular biology of the Ets family of transcription factors. Gene *303*, 11–34.

Omori, A., Tanabe, O., Engel, J.D., Fukamizu, A., and Tanimoto, K. (2005). Adult stage γ-globin silencing is mediated by a promoter direct repeat element. Mol. Cell. Biol. *25*, 3443–3451.

Papa, F.R. (2012). Endoplasmic reticulum stress, pancreatic β-cell degeneration, and diabetes. Cold Spring Harb. Perspect. Med. *2*, a007666.

Park, S.G., Park, H.S., Jeong, I.K., Cho, Y.M., Lee, H.K., Kang, Y.-S., Kim, S., and Park, K.S. (2010). Autoantibodies against aminoacyl-tRNA synthetase: novel diagnostic marker for type 1 diabetes mellitus. Biomarkers *15*, 358–366.

Perry, R.P., and Kelley, D.E. (1970). Inhibition of RNA synthesis by actinomycin D: characteristic dose-response of different RNA species. J. Cell. Physiol. *76*, 127–139.

Pino, M.F., Ye, D.Z., Linning, K.D., Green, C.D., Wicksteed, B., Poitout, V., and Olson, L.K. (2005). Elevated glucose attenuates human insulin gene promoter activity in INS-1 pancreatic β-cells via reduced nuclear factor binding to the A5/core and Z element. Mol. Endocrinol. *19*, 1343–1360.

Poitout, V., and Robertson, R.P. (2008). Glucolipotoxicity: fuel excess and beta-cell dysfunction. Endocr. Rev. *29*, 351–366.

Prentki, M., Matschinsky, F.M., and Madiraju, S.R. (2013). Metabolic signaling in fuel-induced insulin secretion. Cell Metab. *18*, 162–185.

Rhodes, C.J. (2005). Type 2 diabetes—a matter of beta-cell life and death? Science *307*, 380–384.

Robinson, M.D., McCarthy, D.J., and Smyth, G.K. (2010). edgeR: a Bioconductor package for differential expression analysis of digital gene expression data. Bioinformatics *26*, 139–140.

Ron, D. (2002). Translational control in the endoplasmic reticulum stress response. J. Clin. Invest. *110*, 1383–1388.

Sandelin, A., and Wasserman, W.W. (2005). Prediction of nuclear hormone receptor response elements. Mol. Endocrinol. *19*, 595–606.

Sander, M., Griffen, S.C., Huang, J., and German, M.S. (1998). A novel glucose-responsive element in the human insulin gene functions uniquely in primary cultured islets. Proc. Natl. Acad. Sci. U S A *95*, 11572–11577.

Scheuner, D., Vander Mierde, D., Song, B., Flamez, D., Creemers, J.W., Tsukamoto, K., Ribick, M., Schuit, F.C., and Kaufman, R.J. (2005). Control of mRNA translation preserves endoplasmic reticulum function in beta cells and maintains glucose homeostasis. Nat. Med. *11*, 757–764.

Schmidt, E.K., Clavarino, G., Ceppi, M., and Pierre, P. (2009). SUnSET, a nonradioactive method to monitor protein synthesis. Nat. Methods *6*, 275–277.

Schneider, R.K., Schenone, M., Ferreira, M.V., Kramann, R., Joyce, C.E., Hartigan, C., Beier, F., Brümmendorf, T.H., Germing, U., Platzbecker, U., et al. (2016). Rps14 haploinsufficiency causes a block in erythroid differentiation mediated by S100A8 and S100A9. Nat. Med. *22*, 288–297.

Shanik, M.H., Xu, Y., Skrha, J., Dankner, R., Zick, Y., and Roth, J. (2008). Insulin resistance and hyperinsulinemia: is hyperinsulinemia the cart or the horse? Diabetes Care *31* (*Suppl 2*), S262–S268.

Sonenberg, N., and Hinnebusch, A.G. (2009). Regulation of translation initiation in eukaryotes: mechanisms and biological targets. Cell *136*, 731–745.

Støy, J., Edghill, E.L., Flanagan, S.E., Ye, H., Paz, V.P., Pluzhnikov, A., Below, J.E., Hayes, M.G., Cox, N.J., Lipkind, G.M., et al.; Neonatal Diabetes International Collaborative Group (2007). Insulin gene mutations as a cause of permanent neonatal diabetes. Proc. Natl. Acad. Sci. U S A *104*, 15040–15044.

Sulic, S., Panic, L., Barkic, M., Mercep, M., Uzelac, M., and Volarevic, S. (2005). Inactivation of S6 ribosomal protein gene in T lymphocytes activates a p53-dependent checkpoint response. Genes Dev. *19*, 3070–3082.

Szabat, M., Page, M.M., Panzhinskiy, E., Skovsø, S., Mojibian, M., Fernandez-Tajes, J., Bruin, J.E., Bround, M.J., Lee, J.T., Xu, E.E., et al. (2016). Reduced insulin production relieves endoplasmic reticulum stress and induces β cell proliferation. Cell Metab. *23*, 179–193.

Tanabe, O., McPhee, D., Kobayashi, S., Shen, Y., Brandt, W., Jiang, X., Campbell, A.D., Chen, Y.T., Chang, Cs., Yamamoto, M., et al. (2007). Embryonic and fetal beta-globin gene repression by the orphan nuclear receptors, TR2 and TR4. EMBO J. *26*, 2295–2306.

Taneera, J., Lang, S., Sharma, A., Fadista, J., Zhou, Y., Ahlqvist, E., Jonsson, A., Lyssenko, V., Vikman, P., Hansson, O., et al. (2012). A systems genetics approach identifies genes and pathways for type 2 diabetes in human islets. Cell Metab. *16*, 122–134.

Thomas, G., Jacobs, K.B., Yeager, M., Kraft, P., Wacholder, S., Orr, N., Yu, K., Chatterjee, N., Welch, R., Hutchinson, A., et al. (2008). Multiple loci identified in a genome-wide association study of prostate cancer. Nat. Genet. *40*, 310–315.

Tiku, V., Jain, C., Raz, Y., Nakamura, S., Heestand, B., Liu, W., Späth, M., Suchiman, H.E.D., Müller, R.U., Slagboom, P.E., et al. (2017). Small nucleoli are a cellular hallmark of longevity. Nat. Commun. *8*, 16083.

Tornovsky-Babeay, S., Dadon, D., Ziv, O., Tzipilevich, E., Kadosh, T., Schyr-Ben Haroush, R., Hija, A., Stolovich-Rain, M., Furth-Lavi, J., Granot, Z., et al. (2014). Type 2 diabetes and congenital hyperinsulinism cause DNA double-strand breaks and p53 activity in β cells. Cell Metab. *19*, 109–121.

Vangipurapu, J., Stančáková, A., Kuulasmaa, T., Kuusisto, J., and Laakso, M. (2015). Both fasting and glucose-stimulated proinsulin levels predict hyperglycemia and incident type 2 diabetes: a population-based study of 9,396 Finnish men. PLoS ONE *10*, e0124028.

Walter, P., and Blobel, G. (1983). Disassembly and reconstitution of signal recognition particle. Cell *34*, 525–533.

Wang, J., Takeuchi, T., Tanaka, S., Kubo, S.K., Kayo, T., Lu, D., Takata, K., Koizumi, A., and Izumi, T. (1999). A mutation in the insulin 2 gene induces diabetes with severe pancreatic beta-cell dysfunction in the Mody mouse. J. Clin. Invest. *103*, 27–37.

Wang, W., Nag, S., Zhang, X., Wang, M.H., Wang, H., Zhou, J., and Zhang, R. (2015). Ribosomal proteins and human diseases: pathogenesis, molecular mechanisms, and therapeutic implications. Med. Res. Rev. *35*, 225–285.

Ward, W.K., LaCava, E.C., Paquette, T.L., Beard, J.C., Wallum, B.J., and Porte, D., Jr. (1987). Disproportionate elevation of immunoreactive proinsulin in type 2 (non-insulin-dependent) diabetes mellitus and in experimental insulin resistance. Diabetologia *30*, 698–702.

Warner, J.R., and McIntosh, K.B. (2009). How common are extraribosomal functions of ribosomal proteins? Mol. Cell *34*, 3–11.

Weir, G.C., and Bonner-Weir, S. (2004). Five stages of evolving beta-cell dysfunction during progression to diabetes. Diabetes *53* (*Suppl 3*), S16–S21.

Winnay, J.N., Dirice, E., Liew, C.W., Kulkarni, R.N., and Kahn, C.R. (2014). p85α deficiency protects β-cells from endoplasmic reticulum stress-induced apoptosis. Proc. Natl. Acad. Sci. U S A *111*, 1192–1197.

Wiśniewski, J.R., Zougman, A., and Mann, M. (2009). Combination of FASP and StageTip-based fractionation allows in-depth analysis of the hippocampal membrane proteome. J. Proteome Res. *8*, 5674–5678.

Wu, Y., Byrne, E.M., Zheng, Z., Kemper, K.E., Yengo, L., Mallett, A.J., Yang, J., Visscher, P.M., and Wray, N.R. (2019). Genome-wide association study of medication-use and associated disease in the UK Biobank. Nat. Commun. *10*, 1891.

Yang, M., Dai, J., Jia, Y., Suo, L., Li, S., Guo, Y., Liu, H., Li, L., and Yang, G. (2014). Overexpression of juxtaposed with another zinc finger gene 1 reduces proinflammatory cytokine release via inhibition of stress-activated protein kinases and nuclear factor-κB. FEBS J. *281*, 3193–3205.

Yang, H., He, J., Xu, X.L., Jiang, J., He, C.Q., and Ma, H.M. (2015). Molecular characterization and tissue expression profile analysis of the porcine JAZF1 gene. Genet. Mol. Res. *14*, 542–551.

Yoshioka, M., Kayo, T., Ikeda, T., and Koizumi, A. (1997). A novel locus, Mody4, distal to D7Mit189 on chromosome 7 determines early-onset NIDDM in nonobese C57BL/6 (Akita) mutant mice. Diabetes *46*, 887–894.

Yu, G., Wang, L.-G., Han, Y., and He, Q.-Y. (2012). clusterProfiler: an R package for comparing biological themes among gene clusters. OMICS *16*, 284–287.

Yuan, L., Luo, X., Zeng, M., Zhang, Y., Yang, M., Zhang, L., Liu, R., Boden, G., Liu, H., and Ma, Z.A. (2015). Transcription factor TIP27 regulates glucose homeostasis and insulin sensitivity in a PI3-kinase/Akt-dependent manner in mice. Int. J. Obesity *39*, 949–958.

Zeggini, E., Scott, L.J., Saxena, R., Voight, B.F., Marchini, J.L., Hu, T., de Bakker, P.I., Abecasis, G.R., Almgren, P., Andersen, G., et al.; Wellcome Trust Case Control Consortium (2008). Meta-analysis of genome-wide association data and large-scale replication identifies additional susceptibility loci for type 2 diabetes. Nat. Genet. *40*, 638–645.

Zhang, Y., and Lu, H. (2009). Signaling to p53: ribosomal proteins find their way. Cancer Cell *16*, 369–377.

Zhang, Y., Liu, T., Meyer, C.A., Eeckhoute, J., Johnson, D.S., Bernstein, B.E., Nusbaum, C., Myers, R.M., Brown, M., Li, W., and Liu, X.S. (2008). Model-based analysis of ChIP-Seq (MACS). Genome Biol. *9*, R137.

Zhou, X., Hao, Q., Liao, J., Zhang, Q., and Lu, H. (2013). Ribosomal protein S14 unties the MDM2-p53 loop upon ribosomal stress. Oncogene *32*, 388–396.

Zmuda, E.J., Powell, C.A., and Hai, T. (2011). A method for murine islet isolation and subcapsular kidney transplantation. J. Vis. Exp. *50*, 2096.

STAR★METHODS

KEY RESOURCES TABLE

REAGENT or RESOURCE	SOURCE	IDENTIFIER
Antibodies		
Monoclonal Rabbit Anti-Jazf1	This paper	N/A
Monoclonal Mouse Anti-Jazf1	Santa Cruz	Cat# sc-376503, RRID: AB_11149923
Polyclonal Rabbit Nr2c2	Sigma	Cat#HPA006313, RRID: AB_1079503
Monoclonal Rabbit Anti-Phospho eIF2α (ser51)	Cell signaling	Cat#3398, RRID: AB_10829234
Monoclonal Rabbit Anti-eIF2α	Cell signaling	Cat# 5324, RRID: AB_10692650
Polyclonal Rabbit Anti-Phospho Perk (Thr981)	Santa Cruz	Cat# sc-32577, RRID: AB_2293243
Monoclonal Rabbit Anti-BiP	Cell signaling	Cat#3177, RRID: AB_2119845
Monoclonal Mouse Anti-Ki67	BD Biosciences	Ca#556003, RRID: AB_396287
Monoclonal Rat Anti-BrdU	Abcam	Cat#ab6326, RRID: AB_305426
Polyclonal Rabbit Anti-Cleaved Caspase 3	Cell Signaling	Cat#9661, RRID: AB_234118
Polyclonal Rabbit Anti-phospho p53 (Ser15)	Cell Signaling	Cat#12571S, RRID: AB_2714036
Monoclonal Mouse Anti-p53	Santa Cruz	Cat#sc-126 RRID: AB_628082
Monoclonal Mouse Anti-γ-Tubulin	Sigma	Cat#T6557, RRID: AB_477584
Monoclonal Rabbit Anti-β-Actin	Cell Signaling	Cat#4970, RRID: AB_2223172
Monoclonal Rabbit Anti-P21	Abcam	Cat#ab109199, RRID: AB_10861551
Monoclonal Mouse Anti-Puromycin	Merck Millipore	Cat#MABE343, RRID: AB_2566826
Polyclonal Rabbit Anti-Myc-tag	Cell Signaling	Cat#2272, RRID: AB_10692100
Monoclonal Mouse Anti-Mdm2	Santa Cruz	Cat#sc-965, RRID: AB_627920
Polyclonal Guinea Pig Anti-Insulin	Dako	Cat#A056401 RRID: AB_2617169
Hoechst 33342	Thermo Fischer Scientific	Cat#H3570
Chemicals, Peptides, and Recombinant Proteins		
D-glucose anhydrous	Sigma	Cat#49139
BrdU	Sigma	Cat# B5002
Insulin solution	Sigma	Cat#I9278
Histopaque-1077	Sigma	Cat#10771
Liberase	Sigma	Cat#05401127001
Lipofectamine 2000	Invitrogen	Cat#11668500
Lipofectamine RNAiMAX	Invitrogen	Cat#13778-075
Trypsin	Promega	Cat#V5111
Phosphatase inhibitor	Thermo Fisher	Cat# 78427
Protease Inhibitor	Sigma	Cat#5056489001
Actinomycin D	Sigma	Cat#A1410
Puromycin	Sigma	Cat#P8833
Thapsigargin	Sigma	Cat#T9033
Cycloheximide	Sigma	Cat#C4859
Sucrose	Sigma	Cat#84100
Anti-HA Magnetic Beads	Thermo Fisher	Cat#88836
IL-1β	Sigma	Cat#I5271
TNF-α	Sigma	Cat#T7539
Interferon-γ	Sigma	Cat#I3265
Sodium Palmitate	Sigma	Cat#P9767
BSA (Fatty acid Free)	Sigma	Cat#A8806

(*Continued on next page*)

Continued

REAGENT or RESOURCE	SOURCE	IDENTIFIER
γ32P-ATP	Perkin Elmer	NEG035C00MC
Nitrocellulose membrane	Perkin Elmer	NBA083C001EA
Amersham Hybond-N+	GE healthcare	RPN2023B
Commercial Assays		
Insulin ELISA	ALPCO	Cat#80-INSRTU-E10-AL
Proinsulin ELISA	Mercodia	Cat#10-1232-01
TUNEL Assay	Millipore	Cat#S7165
Deposited Data		
RNA sequencing	This paper	PRJNA595139
ChIP sequencing	This paper	PRJNA595471
Experimental Models: Cell Lines		
MIN6	Provided by Dr. C. Wolheim	N/A
INS1E 832/13 with low passage number	Provided by Boehringer Ingelheim GmbH	N/A
ENDOC-βH2	Univercell biosolutions	N/A
Experimental Models: Organisms/Strains		
Mouse.C57BL/6.Jazf1:tm1a(EUCOMM) Wtsi	KOMP repository	Clone ID: 637131
Mouse. B6.RIP-Cre	Provided by Prof. P. Herrera	N/A
FLPe knock in/ROSA26 (FLP1 Deleter)	The Jackson Lab	Stock No:009086
Mouse Diabetic db/db B6.BKS(D)-*Lepr^{db}*/J	The Jackson Laboratory	Stock No. 000697
Mouse.Akita mice: C57BL/6-Ins2^{Akita}/J	The Jackson Laboratory	JAX: 003548
Oligonucleotides		
siRNA: Human Jazf1	Dharmacon	L-018012-01-0005
siRNA: Mouse Jazf1	Dharmacon	L-055638-01-0005
siRNA: Rat Jazf1	Dharmacon	L-108949-00-0005
siRNA: Srp54a	Dharmacon	L-099583-02-0005
siRNA: Dars	Dharmacon	L-096367-02-0005
siRNA: Gars	Dharmacon	L-095034-02-0005
siRNA: Rpl10	Dharmacon	L-095634-02-0005
siRNA: Scramble	Dharmacon	D-001810-10
Sequence-Based Reagents		
Primers for PCR, RT-qPCR and probes for Northen blot analysis are listed in Table S4	This paper	N/A
Recombinant DNA		
Jazf1 adenovirus: Ad: Jazf1-HA-tagged	This paper	N/A
Gfp adenovirus: Ad:GFP	This paper	N/A
Nop56 (Myc-DDK-tagged)	Origene	MR209091
Tsr3 (Myc-DDK-tagged)	Origene	MR204683
Rps2 (Myc-DDK-tagged)	Origene	MR204027
Rps11 (Myc-DDK-tagged)	Origene	MR216516
Rps14 (Myc-DDK-tagged)	Origene	RC203889
Rps15 (Myc-DDK-tagged)	Origene	MR200959
Rps20 (Myc-DDK-tagged)	Origene	MR200561
Rpl10a (Myc-DDK-tagged)	Origene	MR200782
Rpl12 (Myc-DDK-tagged)	Origene	MR201323
Rpl13 (Myc-DDK-tagged)	Origene	MR202263
Rpl13a (Myc-DDK-tagged)	Origene	MR202103

(*Continued on next page*)

Continued

REAGENT or RESOURCE	SOURCE	IDENTIFIER
Software and Algorithms		
Prism 8	GraphPad	https://www.graphpad.com/scientific-software/prism/
Progenesis QI for proteomics	Nonlinear Dynamics	http://www.nonlinear.com/progenesis/qi-for-proteomics/
Fiji	Fiji ImageJ	https://fiji.sc/
Integrative Genomics Viewer (IGV) tool version 2.4	Robinson et al., 2010	N/A
(Enrichr) Enrichment analysis	Kuleshov et al., 2016	http://amp.pharm.mssm.edu/Enrichr/
MEME suite	Machanick and Bailey 2011	N/A
NHR-scan	Sandelin et al.,2004	N/A
FGCZ Heatmap	Generated by SUSHI	http://fgcz-shiny.uzh.ch/fgcz_heatmap_app/
Other		
Normal Chow Diet	KLIBA NAFAG	3437
High Fat Diet	SAFE	260HF

RESOURCE AVAILABILITY

Lead Contact

Further information and requests for resources and reagents should be directed to and will be fulfilled by the Lead Contact, MS (stoffel@biol.ethz.ch).

Materials Availability

The *Jazf1*$^{fl/fl}$ mouse line (Jazf1tm1a (EUCOMM) Wtsi) is deposited at the European Conditional Mouse Mutagenesis Program Eucomm.

Data and Code Availability

The accession numbers for the RNA-seq and ChIP-seq data reported in this paper are ArrayExpress: PRJNA595139 and ArrayExpress: PRJNA595471, respectively.

EXPERIMENTAL MODEL AND SUBJECT DETAILS

Mouse models

All animals were housed in a pathogen-free animal facility at the Institute of Molecular Health Sciences at ETH Zurich. Mice were maintained on a 12-h light/ dark cycle (lights on from 6:00 to 18:00). Mice were given *ad libitum* access to a standard laboratory chow or HFD (SAFE, 260HF) containing 20% protein, 36% lipids and 36.7% carbohydrate, and water. Male mice were used for all experiments shown (except Akita) and the age of mice was above 8-12 weeks unless otherwise indicated in Figures. All mice were maintained on a pure C57BL/6N background. Genotypings of *Jazf1*$^{fl/fl}$, *Rip-Cre* or *Akita* mice were performed by PCR with primers listed in Table S4. All animal experiments were in accordance with institutional guidelines and approved by the kantonale Veterinäramt Zürich.

Generation of βJazf1KO mice

Mouse.C57BL/6.Jazf1:tm1a(EUCOMM)Wtsi

Mice carrying the Jazf1 mutation (Jazf1tm1a (EUCOMM) Wtsi) were obtained from the Knockout Mouse Project (KOMP) repository (https://www.komp.org/ProductSheet.php?cloneID=637131). Briefly, Jazf1tm1a (EUCOMM)Wtsi mice contain an IRES:LacZ trapping cassette and a floxed promoter-driven neo cassette inserted. Jazf1tm1a(EUCOMM)Wtsi mice were initially crossed with Flp-1 trangenic line (Jackson Lab) to remove the FRT-flanked lacZ-neo cassette, converting the ''knockout-first'' allele to a conditional allele (*Jazf1*$^{fl/fl}$). To generate the beta cell-specific knockout animals *(βJazf1KO)*, Jazf1 floxed mice were crossed with RIP-Cre transgenic mice leading to exon 3 deletion. RIP-Cre Jazf1 KO mice were maintained on a C57BL/6N background.

Rip-Cre mice (Tg(Ins2-cre)23Herr) were kindly provided by P. Herrera. A 0.6 kb fragment containing the rat insulin promoter was adjoined to the Cre recombinase coding sequence to drive expression in pancreatic cells. The insertion of the transgene is unknown.

Animal procedures

High fat diet

Male mice were fed a HFD starting at 5 weeks old for 12 weeks.

Blood glucose measurements IPGTT and BrdU injection

Mice were fasted for 6 h and injected intraperitoneally with D-glucose (Sigma, 49139) solution (2.5 g/kg dose for chow diet mice and 1.5 g/kg for HFD mice) for IPGTT experiment. Blood glucose values were measured with a Bayer Contour XT glucometer at 0, 15, 30, 45, 60, and 120 min after injection.

For β-cell proliferation study, mice were injected intraperitoneally with Brdu (100 mg/kg) (Sigma, B5002) for 2 days before mouse dissection.

Cell culture and transfections

INS1E

Initial stocks of the clonal INS1E 832/13 were provided by Boehringer Ingelheim GmbH with passage number 85 (P85) and cultured in RPMI 1640 supplemented with 11.1 mM D-glucose, 10% (v/v) fetal bovine serum (FBS), 10 mM HEPES, 1 mM Pyruvate, 50 μM beta-mercaptoethanol, 2 mM Glutamax (GlutaMAX, Invitrogen) and 10,000 units/mL penicillin and 10 mg/mL streptomycin. Cells were incubated at 37°C in 5% CO_2, 95% air. All experiments used cells harvested between passages P88-90.

MIN6

The initial stock of the clonal MIN6 cell line was obtained by Prof. C. Wolheim. Cells were cultured in DMEM supplemented with 20% (v/v) FBS, 2 mM Glutamax (GlutaMAX, Invitrogen), 30 μM beta-mercaptoethanol and 10,000 units/mL penicillin and 10 mg/mL streptomycin.

EndoC-βH2:

Cells were obtained from Univercell biosolutions company. Cells were culture in complete medium culture (Reference: OPTIβ1 ®)

INS1E, MIN6 and EndoC-βH2 cell lines were authenticated in-lab by performing GSIS assays and by RT-PCR of beta-cell specific genes. Cells are routinely tested twice annually for the presence of Mycoplasma and found negative.

INS1E, **MIN6, EndoC-βH2 cells** were maintained at 37 C in a humidified incubator with 5% CO2 in air.

Expression and purification of recombinant Zinc finger domains

To prepare pure GST proteins, BL21(DE3) cells were grown at 37 C in a fermentor to an A600 of ~0.5. Protein expression was induced with isopropyl 1-thio-β-D-galactopyranoside (0.5 mM) and protein allowed to accumulate for an additional 4h. Following centrifugation, a pellet from 6 l of culture was resuspended in ZnF buffer (10 mM NaH_2PO_4, pH 7.4, 150 mM NaCl, 5 mM β-ME, 10 μM $ZnCl_2$). All purification steps were performed at 4°C. Bacteria were lysed by sonication and the lysate was centrifuged (40,000 x g for 30 min) to remove insoluble debris. GST-ZF23 and GST-JAZF1 was recovered from the lysate by affinity chromatography using a GSTPrep FF 16/10 affinity column (Amersham Biosciences). Bound protein was washed with 10 column volumes of ZnF buffer and eluted with 20 mM glutathione in 50 mM HEPES, pH 7.4, 5 mM β-ME, and 10 μM $ZnCl_2$. Purification of MBP-fusion proteins were done in a similar manner.

Antibody production

Protein fragments corresponding to amino acids 1-243 and 170-243 of JAZF1 fused to glutathione *S*-transferase (GST) were expressed, purified using glutathione Sepharose 4B (Amersham Biosciences) and used to raise JAZF1- N64 antibodies. JAZF1 antibodies were raised in rabbits immunized seven times with 500 μg of the GST-fusion protein (Davids Biotechnoligie GmbH (Germany)). JAZF1 specific antibodies were purified from 50 mL of serum in PBS on a Sepharose 2B column containing identical JAZF1 fragments fused to maltose-binding protein (MBP) coupled to CNBr activate Sepharose 2B beads and eluted with 0.1 M glycine (pH 2.5).

Recombinant adenoviruses

Recombinant Adenovirus were generated by cloning the murine Jazf1 cDNA into pVQAd CMV K-NpA (pVQAd, Viraquest). Ad-Ctrl was based on the same vector backbone (with a GFP) but lacked the *Jazf1* transgene.

For virus infection experiments, cells were infected with Ad-Jazf1 or Ad-GFP at a MOI 5 for cells and a MOI 20 for dispersed islets.

Human islets and pancreatic sections

Human islets were obtained from Prodo Laboratories Inc. Pancreatic biopsy specimens from Caucasian patients were obtained postmortem at the University Hospital, Zurich. Pancreatic specimens were formaldehyde fixed for histopathological examination. Informed consent was obtained in accordance with the regulations of the Ethics Committee of the Canton Zurich.

Isolated Islets were from healthy and T2D donors (see table below). The islet preparation of donors consisted of 2,500 – 10,000 islet equivalents with a purity of >80% and a viability of >90%. Pancreatic islets were handpicked under a microscope and cultured in CMRL-1066 medium containing 5.6 mM glucose, 10% FBS, 100 IU/ml penicillin/streptomycin and glutamax.

Donor	Gender	Age	Diagnosis	Cause of death	BMI
1	M	29	N	Stroke	42.2
2	M	45	T2D	Stroke	27.3
3	M	60	N	Stroke	27.4
4	F	53	N	CVD	32
5	M	48	T2D	Gunshot	43.7
6	M	43	T2D	Stroke	27.6
7	M	59	T2D	Stroke	32.5
8	M	37	N	Stroke	25.4
9	M	57	N	Stroke	29.4
10	F	41	T2D	Stroke	43.1

Mouse pancreatic islet

Mouse pancreatic islets were isolated from male mice as previously described (Zmuda et al., 2011) with slight modifications. A total of 2 mL of Liberase (5 mg/ml) (Sigma 05401127001, diluted in HBSS buffer, GIBCO, 14170-112) was injected through the common bile duct to perfuse the whole pancreas. The perfused pancreas was dissected and incubated at 37°C for 17 min. Digested exocrine cells and intact islets were separated via centrifugation (2400 × rpm for 20 min with very slow acceleration and no braking) over Histopaque-1077 (Sigma, 10771), and intact islets were manually picked under the microscope. Islets were cultured in RPMI 1640 with 10% FBS and 100 U/ml penicillin/streptomycin.

METHOD DETAILS

Immunohistochemistry and β-cell mass measurements

Whole pancreas or pancreatic buds were fixed with 4% paraformaldehyde (PFA) and embedded in paraffin, and the cut sections were antigen-retrieved by boiling them in citrate buffer (10 mM Citric Acid, 0.05% Tween 20, pH 6.6). Cells or dispersed islets were fixed with 2% PFA for 15 min. The sections or cells were permeabilized and blocked in PBS containing 0.1% Triton X-100, 1% BSA and 5% goat serum. Primary antibody binding was performed overnight at 4°C, while secondary antibody incubation was carried out at room temperature (21°C) for 1h. Leica TCS SP8 confocal microscope was used for fluorescent imaging.

For β-cell mass, Ki-67 or BrdU labeling and Tunel assay, 3.5 mm sections were cut and 5 sections that were at least 500mm apart were taken from each mouse and stained for insulin and DNA (Hoechst). Entire pancreatic sections were scanned using Panoramic 250 Slide scanner (3D Histech). The fraction of insulin positive area compared to total pancreatic area (stained with Hoechst) was analyzed using Fiji software (https://fiji.sc/), and β-cell mass was calculated by multiplying this fraction by the initial pancreatic weight.

For nucleolar and nuclear area, MIN6 cells are transfected with Jazf1 or scramble siRNAs for 48h. Cells are fixed with 2% PFA for 15 min then are permeabilized and blocked in PBS containing 0.1% Triton X-100, 1% BSA and 5% goat serum. The nucleolus was detected by Fibrillarin antibody, and the nucleus was detected by Hoechst staining and fluorescence images were observed using a Zeiss Apotome 2 microscope. The area of the nucleolar and nuclear regions was quantified using Fiji software (https://fiji.sc/).

For cell proliferation assay, INS1E cells were transfected by a reverse transfection with Jazf1 or scramble siRNAs for 48 h. Cells were fixed with 2% PFA for 15 min, then permeabilized and blocked in PBS containing 0.1% Triton X-100, 1% BSA and 5% goat serum. The nucleus was detected by Hoechst staining and fluorescence images were observed using a Zeiss Apotome 2 microscope.

Insulin and Proinsulin

To determine mouse serum insulin or Proinsulin levels, blood was obtained from the tail vein and centrifuged for serum separation. Insulin was measured by Insulin ELISA Kit (ALPCO, 80-INSRTU-E10-AL) and Proinsulin was measured by ELISA Kit (Mercodia, 10-1232-01). To measure total pancreatic insulin content, insulin was extracted by acid-ethanol buffer (HCl:Ethanol 1:49, 0.1% Triton) from total pancreas. For islet insulin content, insulin was extracted by acid-ethanol buffer (HCl:Ethanol 1:49, 0.1% Triton) from 80 size matched islets. Hormones were then assessed by Insulin ELISA Kit.

Dispersed islets experiments

Islets were digested by 0.05% trypsin at 37°C for 5 min, and then centrifuged and resuspended. Cells were seeded into a 96-well plate which was coated overnight with medium from 804G cell line culture (Langhofer et al., 1993). Dispresed islets were cultured in low or high glucose. Leica TCS SP8 confocal microscope was used for fluorescent imaging.

Transfections

For knockdown experiments cells, INS1E or MIN6 were plated in 6 well plates and transfected the next day at 60%–70% confluency. For each well to be transfected, an RNAi duplex-Lipofectamine® RNAiMAX complexes was prepared as follows: 30 nM (final concentration) RNAi duplex was diluted in Opti-MEM® reduced Serum Medium. 7 μl of Lipofectamine® RNAiMAX was diluted in Opti-MEM®, and mixed gently. The diluted RNAi duplex was combined the diluted Lipofectamine® RNAiMAX and mixed gently. The RNAi duplex-Lipofectamine® RNAiMAX complexes were incubated for 10 min at room temperature before transferring them to each well containing cells. The medium was changed after 6 h and cells were incubated for 48 h at 37°C in a CO_2 incubator.

For transient plasmid transfections INS1E or MIN6 cells were plated in 6 well plates with growth medium without antibiotics overnight and transfected the next day at 60%–80% confluency. Using a DNA (ug) to Lipofectamine 2000 (ul) ration of 1:3. The liquid was gently mixed by rocking the plate back and forth and incubated at 37°C in a CO_2 incubator. The medium was changes after 6 h and incubated for 42 h before harvesting the cells. Successful transfection and expression of vector in cells was assessed by RT-qPCR and or western blotting.

Treatment with reagents

Cells or islets are treated with 5nM of Actinomycin D (Ribosome stress) or 500 nM thapsigargin (ER stress), cytokines cocktail (10 ng/ml IL-1β, 100 ng/ml IFN-γ and 25 ng/ml TNF-α), low glucose (3mM), high glucose (15mM) or chronic high glucose (25mM). The duration of treatments is indicated in the figure legends for each experiment.

Stress induction of human islets with glucose, palmitate, and cytokines

Islets were from donors. The islet preparation of donors consisted of 2,500 islet equivalents with a purity of >80% and a viability of >90%. Pancreatic islets were handpicked under a microscope and cultured in CMRL-1066 medium containing 5.6 mM glucose, 10% FBS, 100 IU/ml penicillin/streptomycin and glutamax; then islets were challenged with 25 mM glucose, cytokines (10 ng/ml IL-1β, 100 ng/ml IFN-γ and 25 ng/ml TNF-α) and 100 uM of palmitate-BSA conjugate. Medium was renewed every 24 h. Islets were collected for experiments after 72 h.

RNA isolation and quantification

TRIzol reagent (Invitrogen, 15596-026) was used for RNA isolation according to the manufacturer's protocol. RNA was reverse transcribed using High Capacity cDNA Reverse Transcription Kit (Applied Biosystems, 4368813). Quantitative PCR was performed in an LC480 II Lightcycler (Roche) and using gene specific primers and Sybr Fast 2x Universal Master mix (Kapa biosystems, KK4611). Results were normalized to 36b4 or Gapdh mRNA levels. The sequences of primers pairs of respective transcripts are shown in Table S4.

Northern blot

Total RNA from indicated cells or islets were extracted by TRIzol (Invitrogen). RNA samples (3-5μg) were heated in RNA loading buffer contains 62.5% deionized formamide, 1.14 M formaldehyde, 200 μg/ml bromphenol blue, 200 μg/ml xylene cyanole, in MOPS-EDTA-sodium acetate at 1.25x working concentration (Sigma-Aldrich R1386) and were electrophoresed in 0.8% formaldehyde-agarose gels (0.8 % agarose – 2.2 M formaldehyde gel) in 1XMOPS buffer at 4∼5 V/cm and transferred onto Hybond N+ membranes (Amersham) with 10 x SSC. ETS, ITS1 and ITS2 probes (sequences indicated in Table S4) used to generate α-^{32}P dCTP-labeled probes. Probes were purified over nucleotide purification columns (Zymo Research) prior to hybridization. Membranes were prehybridized for 1 hr at 65°C in 50% formamide, 5 × SSPE, 5 × Denhardt's solution, 1% w/v SDS, 200 μg/ml salmon sperm DNA. The ^{32}P-labeled oligonucleotide probe was added and incubated overnight at 50°C. Blots were developed on PhosphorImager screens and developed on a Typhoon Imager. Northern blot quantification based on densitometry of bands was performed in ImageJ.

Luciferase assay

Wild-type, mutant, and deletion of NR2C2 element in the promoters region of the human *Ins*, rat *Rps14* and *Rpl10* genes were generated by *de novo* DNA synthesis (Gene Universal) and cloned to a luciferase reporters (pGL4.25[luc2CP/minP] Vector (Promega cat#: E8411).

INS1E or ENDOC-βH2 cells were grown in until cells were 60%–80% confluent. Cells were cultured in 96-well plates and transfected with 30 nM si-RNA of si-Jazf1 or si-Scramble. After 24h, cells are transfected with 200 ng of a luciferase reporters vector under the control of the wild-type and mutants promoters and with 100 ng of pRL *Renilla* luciferase control reporter vector (Promega cat#: E2411) as an internal control for transfection efficiency. The complex of DNA/lipofectamine 2000 are used 1:3 ratio. One day after transfection, cells were harvested and assayed using the Dual-Luciferase Reporter Assay System (Promega).

Polysome profiling

MIN6 cells were treated with 0.1 mg/mL cycloheximide (Sigma-Aldrich) for 5 min at 37 °C, washed twice with 0.1 mg/mL cycloheximide in 1X PBS. Polysome lysis buffer composed of 15 mM Tris HCl pH 7.4, 15 mM $MgCl_2$, 300 mM NaCl, 100 μg/mL cycloheximide, 1% Triton X-100, 40 U/μL RNase and protease inhibitors. The lysis buffer was used to resuspend cells, followed by 10 min incubation on ice and 5 min centrifugation at 13,000 rpm at 4 °C. Clear supernatants (1,5mg of protein) from lysed cells were loaded into the 10 to

50% sucrose gradient. After centrifugation for 4h at 32′000 rpm at 4°C in a SW41 rotor (Beckman Coulter), gradients were analyzed at OD254 with a Foxy Jr. Gradient collector (Teledyne Isco).

Proteomic studies

10^7 INS1E cells were used per IP sample. Proteins were extracted by NP-40 buffer with protease inhibitors. Protein samples were digested to peptides with Filter-aided Sample Preparation (FASP) method (Wiśniewski et al., 2009). Peptide enrichment was performed after FASP with Ti-IMAC (Resyn Biosciences, MR-TIM002). Enriched peptides were dissolved in 10 μl LC-MS solvent (3% acetonitrile, 0.1% formic acid) after C18 ZipTip (Millipore, ZTC18S096) desalting.

Mass spectrometry analysis was performed on an Orbitrap Fusion Tribrid mass spectrometer (Thermo Scientific, San Jose, CA), which was connected to an Easy-nLC 1000 HPLC system (Thermo Scientific). Liquid chromatography solvent compositions in channels A and B were 0.1% formic acid in water and 0.1% formic acid in acetonitrile, respectively. 4 μl of the sample in LC-MS solvent was loaded onto a frit column (inner diameter 75 μm, length 15 cm) packed with reverse phase material (C18-AQ, particle size 1.9 μm, pore size 120 Å, Dr. Maisch GmbH, Germany), and separated at a flow rate of 300 nL per min. The following LC gradient was applied: 0 min: 1% buffer B, 80 min: 30% B, 90 min: 50% B, 95 min: 98% B, 100 min: 98% B.

Survey scans were recorded in the Orbitrap mass analyzer in the range of m/z 350-1800, with a resolution of 60000, and AGC target value of 200,000 and a maximum injection time of 50 ms. Higher energy collisional dissociation (HCD) spectra were acquired in the linear ion trap analyzer, using a normalized collision energy of 30%. A maximum injection time of 100 ms, and an AGC target value of 30,000 were applied. The precursor ion isolation width was set to m/z 2,0. Charge state screening was enabled, and only precursor ions with charge states 2-7 were included. The threshold for signal intensities was 5000, and precursor masses already selected for MS/MS acquisition were excluded from further selection during 45 s.

Immunoblot analysis

Cells or islets were collected and lysed by RIPA Buffer (50 mM Tris pH 7.5, 1% NP-40, 0,5% Na-Deoxycholate, 0.1% SDS, 150 mM NaCl, 1 mM EDTA pH 8.0, supplemented with protease and phosphatase inhibitors. Protein concentrations were determined by Bicinchonic Acid (BCA) assay. 30-50 μg of total protein lysates were mixed with Laemmli buffer and boiled for 5 min. 10%–14% SDS-PAGE gel was used for protein separation. Membranes were blocked by 5% milk/TBS-T or 5% BSA/TBS-T (for phosphorylation antibodies) for 1 h after electrotransfer to nitrocellulose membranes (NBA083C001EA, Perkin Elmer) and incubated with appropriate antibodies overnight at 4°C. Membranes were exposed to secondary antibodies for 1 h at room temperature and developed using ECL Western Blotting Substrate (Thermo, 32106). Immunoblotting quantification based on densitometry of bands was performed in ImageJ

Cellular fractionation

Freshly isolated islets were digested with trypsin into single cells and washed with PBS. Cell pellet was re-suspended in Hypotonic Lysis Buffer (HLB, 10 mM HEPES, 1.5 mM $MgCl_2$, 10 mM KCl, 1 mM DTT and fresh protease inhibitor) and incubated on ice for 30 min. 6 μL 10% NP40 per 100 μL HLB was added after the incubation and vortexed for 10 s, then centrifuged immediately for 30 s. Supernatant was saved as cytosolic extract. The nuclei were then washed with 1 mL of HLB to remove any contaminating cytoplasm and re-sedimented. Pellet was re-suspended in Nuclear Lysis Buffer (NLB, 10 Mm HEPES, 100 mM KCl, 3 mM $MgCl_2$, 0.1 mM EDTA, 1 mM DTT and fresh protease inhibitor) and incubated on ice for 30 min. Extra 1/10th volume of 4 M $(NH_4)_2SO_4$ was added over 30 min. Solution was centrifuged and the supernatant was saved as nuclear extract.

Protein concentrations were determined by bicinchoninic acid (BCA) assay and equal amounts of protein were loaded for immunoblotting.

Co-Immunoprecipitation assay

10^7 INS1E cells are used per IP sample. Cells are whased twice in cold 1x PBS. Cells are lysed in NP-40 buffer (20 mM Tris HCl pH 8,137 mM NaCl, 1% NP-40, 2 mM EDTA) for 30 min in ice. Cellular debris were removed by centrifugation at 4°C for 10 min and transfer the supernatant to a new 2 mL tube. Save 4% of the lysate as an input control, the remaining lysate were adjusted to the volume of 1.5 mL with pre-cold lysis buffer. Add 70 ul of anti HA magnetics beads against the HA tagged Jazf1 protein. Incubate the tubes on a tube rotator 4h at 4°C. (same for IgG mouse: negative control). Wash 5 times the beads with the lysis buffer. After washing, resuspend the beads in 30 μL of 2x Laemmli buffer, boil for 5 min, and analyze by immunoblot analysis.

Puromycin analysis

The cells or isolated pancreatic islets were treated with puromycin (1 μg/ml) for 30 min in fresh medium. The cells were lysed and protein synthesis was detected with anti-puromycin antibodies by western blot.

Illumina RNA sequencing

Total RNA was isolated from islets using PicoPure® RNA Isolation Kit (Invitrogen, KIT0204). Sequencing libraries were prepared from 100-500 ng total RNA using the TruSeq RNA Sample Preparation Kit v2 (Illumina) according to the manufacturer's protocol. Briefly, total RNA samples (100–1,000 ng) were polyA selected and reverse transcribed into double-stranded cDNA. Then cDNA samples

were fragmented, end repaired, and polyadenylated before ligation of TruSeq adaptors containing the index for multiplexing fragments on both ends were selectively enriched with PCR. The quality and quantity of the enriched libraries were validated using Qubit (1.0) Fluorometer and the Caliper GX LabChip GX (Caliper Life Sciences). The product is a smear with an average fragment size of approximately 260 bp. The libraries were normalized to 10 nM in Tris-Cl 10 mM, pH 8.5 with 0.1% Tween-20.

The quality of RNA-seq reads were checked with fastqc, which computes various quality metrics for the raw reads. Reads were aligned to the genome and transcriptome with TopHat v. 1.3.3 (https://ccb.jhu.edu/software/tophat/manual.shtml). Before mapping, the low-quality ends of the reads were clipped (three bases from the read start and 10 bases from the read end). TopHat was run with default options. The 'fragment length' parameter was set to 100 bases with a standard deviation of 100 bases. On the basis of these alignments, the distribution of the reads across genomic features was assessed. Isoform expression was quantified with the RSEM algorithm (Li and Dewey 2011) with the option for estimation of the read start position distribution turned on. Transcripts were defined using the Ensemble annotations over protein-coding mRNAs. Differential expression analysis of mapped RNA-seq data were performed using EdgeR (Robinson et al., 2010).The raw sequencing data were deposited at NCBI Sequence Read Archive (SRA, https://www.ncbi.nlm.nih.gov/bioproject/?term=PRJNA595139) and are accessible through the accession number PRJNA595139.

Jazf1 expression in islets from human and mouse T1D model

RNA-seq dataset from islets of human T1D (Mastracci et al.,2018: Accession number GSE102371). RNA-seq dataset from islets of B10.RagKO and NOD.RagKO mice (Dooley et al., 2016: Accession number GSE56507). Array expression data from islets of NOD mice. (Carrero et al., 2013: Accession number GSE41203).

The expression data of individual samples were merged, transcript expression was converted to gene expression and ensembl gene ids were mapped to HGNC symbols. Differential gene expression analysis was carried out by DESeq2.The data were processed using in-house Python and R scripts. The Affymetrix MoGene IDs were annotated to ensembl IDs, gene symbols, chromosome loci etc. by the Biomart R package.

ChIP-Seq assay

10^7 INS1E cells are used per IP. Cells were crosslinked with 1% formaldehyde for 10 min at room temperature, crosslinking was stopped by addition of 2M Glycine (0.125M final concentration) at room temperature for 5 min. Cells are washed twice in cold 1x PBS. Cells are lysed into ice-cold lysis buffer (50 mM Tris-HCl, pH 8.1, 1% SDS, 10 mM EDTA, 1X protease inhibitors) for 1h in ice. Following cell lysis, the samples were sonicated (Bioruptor Plus, Diagenode) to generate fragments of average length of 300-100 base pairs. Cellular debris were removed by centrifugation at 4°C for 10 min (10,000 g), 10 % of the lysate was stored as the source of ''Input'' and the remaining lysate was diluted 8 times in dilution buffer (final concentration: 16.7 mM Tris-HCl, pH 8.1, 0.01 SDS, 1.1% Triton X-100, 1.2 mM EDTA, 16.7 mM NaCl, protease inhibitor), in presence of 70 μL of anti-HA Magnetic beads were then incubated at 4°C with rotating for overnight.

Beads were washed extensively at 4°C in Low salt buffer (20mM Tris-HCl, pH 8.1, 0.1% SDS, 1%Triton X-100, 2mM EDTA, 150 mM NaCl), in High salt buffer (20mM Tris-HCl, pH 8.1, 0.1% SDS, 1%Triton X-100, 2mM EDTA, 500mM NaCl), and in LiCl buffer (10mM Tris-HCl, pH 8.1, 250mM LiCl, 1% NP-40, 1% sodium deoxycholate, 1mM EDTA), and finally in 1ml of TE buffer (10mM Tris-HCl, pH 8.0, 1mM EDTA). The bound chromatin was released from the beads by vortexing at room temperature in 200 μL elution buffer (1% SDS and 100 mM NaHCO3). 1 μL of 10mg/ml RnaseA and 5M NaCl (200mM final concentration) was added to the eluate and incubated O/N at 65°C, and then treated with Proteinase K for 1 hr at 55°C; DNA was purified using QIAGEN PCR purification kit.

ChIP-seq data processing

Short reads generated in this study were deposited at NCBI Sequence Read Archive (SRA, https://www.ncbi.nlm.nih.gov/bioproject/?term=PRJNA595471) and are accessible through the accession number

PRJNA595471. Adaptor sequences and low quality stretches within the reads were removed with TrimGalore (options –illumina, version version 0.4.0, www.bioinformatics.babraham.ac.uk/projects/trim_galore). Reads were then aligned to the rat reference genome (ensembl93) with bowtie2 keeping only unique alignments with a mapping quality greater than 10 (version 2.8.2, Langmead and Salzberg, 2012). For each sample, coverage peaks were identified with MACS (version 2.1.1; Zhang et al., 2008) with a Q-value threshold of 0.05 for the identification of broad peaks. Peaks of the two batch 1 and the four batch 2 replicates were merged with MULTOVL and only peaks identified in at least two batch 1 or at least three batch 2 replicates were kept (version 1.3, options -m 3 -u; Aszódi,2012). Reads overlapping with at least 30 bases with the peaks were counted with featureCounts (version 1.6.0, multiple overlaps allowed, Liao, Smyth, and Shi,2014). Peaks not mapped by at least five reads in any of the samples were excluded from further analyses. Peak regions were mapped to the genomic context (e.g., promoter or intergenic) with Homer (version 4.10, Heinz et al., 2010) and the rn6 annotation.

Differential binding

Variation in sequence counts between IP and control conditions was analyzed with a general linear model in R with the package DESeq2 (version 1.14.1, (Love, Huber, and Anders, 2014)). We first fitted a factor to account for batch effects (~batch + treatment). p

values were adjusted for multiple testing (Benjamini-Hochberg), and peaks with an adjusted p value (false discovery rate, FDR) below 0.05 and a minimal log2 fold-change (i.e., the difference between the log2 transformed, normalized sequence counts) of 0 were considered to be significantly bound by Jaz1. Normalized sequence counts were calculated accordingly with DESeq2 and log2(x+1) transformed.

Functional characterization with GO terms

To functionally characterize genes with a significantly Jaz1-bound peak in their promoter (1 kb up- and downstream of the transcriptional start site), we tested for enrichment of gene ontology (GO) terms with topGO (version 2.28 Alexa, Rahnenführer, and Lengauer, 2006) in conjunction with the GO annotation from Ensembl available through biomaRt (Durinck et al., 2009). Analysis was based on gene counts using the "weight" algorithm with Fisher's exact test (both implemented in topGO). A term was identified as significant if the p value was below 0.05.

Enrichment of KEGG pathways in gene sets was tested with clusterProfiler (version 3.12.0, Yu et al., (2012)) using the gene to pathway mappings available through biomaRt (Durinck et al., 2009) and the package org.Rn.eg.db (version 3.8.2, Carlson, 2019).

Motif discovery

To search for known and novel motifs we used MEME-ChIP and 2 kb sequences centered around significantly Jaz1-bound peaks (version 5.0.2 with the parameters -meme-mod zoops -meme-minw 6 -meme-maxw 30 -meme-nmotifs 10 -dreme-e 0.05 -centrimo-score 5.0 -centrimo-ethresh 10.0, Machanick and Bailey (2011)). The percentage of peaks with a motif similar to CCGGAA was extracted from the CentriMo output (part of the MEME-ChIP pipeline). To further search for the presence of nuclear hormone receptor binding sites in significantly Jaz1-bound peaks in promoter (1 kb up- and downstream of the transcriptional start site) and intergenic regions we used NHRscan with default settings (available at nhrscan.genereg.net, accessed at the 24th of November 2019, Sandelin and Wasserman, 2005).

UK BioBank data processing

The genotype data from rs1635852 (affy30273931) was obtained through UK Biobank application number 48008. The data were extracted and filtered for missing data using in-house scripts implemented with python 3.6 (python.org) and pandas (https://pandas.pydata.org/). The cleaned initial dataset included 241196 participants with the C T genotype, 125147 participants with the T T genotype, 121524 participants with the C C genotype. The diabetic participants were 26740 (5.481% of the whole dataset). We applied general linear model (GLM) to identify the association between the SNPs and phenotypes. In case of continuous phenotypes, GLM with Gaussian link function was used. To analyze binary phenotypes like diabetes, we append GLM with logit link function of binomial distribution. The p values and effect sizes (beta coefficient in case of linear regression and odds ratio in case of logistic regression) were used to assess the magnitude of the SNP effect on a given phenotype.

The Linear Regression used here can be written in the following form:

$$Y = \beta_0 + snp_*\beta_1 + age_*\beta_2 + sex_*\beta_3 + pc1_*\beta_4 + \ldots + pc10_*\beta_{13} + \varepsilon$$

The Logistic Regression we applied may be written in the following form:

$$Y = 1/(1 + \exp - (\beta_0 + \mathrm{snp}_*\beta_1 + \mathrm{age}_*\beta_2 + \mathrm{sex}_*\beta_3 + \mathrm{pc1}_*\beta_4 + \ldots + \mathrm{pc10}_*\beta_{13} + \mathrm{e}))$$

Generalized linear regression analysis was conducted on blood biochemical data (fields: 30630-0.0 Apolipoprotein A, 30640-0.0 Apolipoprotein B, 30690-0.0 Cholesterol, 30740-0.0 Glucose, 30760-0.0 HDL cholesterol, 30750-0.0 Glycated haemoglobin (HbA1c), 30780-0.0 LDL direct, 30870-0.0 Triglycerides), biometric measurements (fields: 21001-0.0 BMI, 23106-0.0 Impedance of whole body) using rs1635852 (affy30273931), age, sex, and genetic Principal Component 1-10 (field 31-0.0 sex, field 21022-0.0 age at recruitment, field 22008-0.0 through 22008-0.10 for genetic principal components) as covariates. The reference genotype used for analysis was C C. The blood biochemical data were available for 467,929 participants, while BMI and impedance for 485887 and 478818 participants, respectively. The additional covariates were included to account for the unwanted source of variation within the population age, sex, ethnic diversity etc.

Logistic regression analysis was conducted on diabetes diagnosed by a doctor (field 2443-0.0, for 487,867 participants) and medication use (Treatment/medication code fields 20003-0.0 through 20003-0.47, for 354,259 participants) using rs1635852 (affy30273931), age, sex, and genetic Principal Component 1-10 (field 31-0.0 sex, field 21022-0.0 age at recruitment, field 22008-0.0 through 22008-0.10 for genetic principal components) as covariates. The reference genotype used for analysis was CC. Medications were grouped according to ATC pharmacological subgroups within therapeutic subgroup A10 (Wu et al., 2019). Medications with different UK Biobank code but identical ATC subcode were grouped in the same category (A10A Insulin, A10BA metformin, A10BB sulfonylurea, A10BG rosiglitazone, A10BD Metformin |Rosiglitazone, A10BF Acarbose, A10BX Meglitinide). The all_diabetes_medication data were obtained by calculating if a participant takes any diabetes medication, regardless of the quantity.

R programming language (https://www.r-project.org/) with tidyverse library (https://www.tidyverse.org/) were used to conduct the statistical analysis.

QUANTIFICATION AND STATISTICAL ANALYSIS

Statistical analysis

Statistical parameters including the exact value of n, precision measures (mean ± SD) and statistical significance are reported in the Figures and Figure Legends. Two-tailed unpaired Student's t test was applied for comparisons between two groups. ANOVA was used on comparisons that involved multiple groups. Statistical differences are indicated as (*: $p < 0.05$; **: $p < 0.01$; ***: $p < 0.001$; ****: $p < 0.0001$). $p < 0.05$ was considered significant. Samples were not systematically blinded before every experiment. Biological or technical replicates are indicated in the figure legends. Statistical analyses were performed using GraphPad Prism 8 software.

ADDITIONAL RESOURCES

None